The presence of pacemaker HCN channels identifies theta rhythmic GABAergic neurons in the medial septum

Viktor Varga[1], Balázs Hangya[1], Kinga Kránitz[1], Anikó Ludányi[1], Rita Zemankovics[1], István Katona[1], Ryuichi Shigemoto[2], Tamás F. Freund[1] and Zsolt Borhegyi[1]

[1]*Department of Cell and Network Neurobiology, Institute of Experimental Medicine of the Hungarian Academy of Sciences, Budapest, Hungary*
[2]*Division of Cerebral Structure, National Institute of Physiological Sciences, Myodaiji, Okazaki 444-8787, Japan*

The medial septum (MS) is an indispensable component of the subcortical network which synchronizes the hippocampus at theta frequency during specific stages of information processing. GABAergic neurons exhibiting highly regular firing coupled to the hippocampal theta rhythm are thought to form the core of the MS rhythm-generating network. In recent studies the hyperpolarization-activated, cyclic nucleotide-gated non-selective cation (HCN) channel was shown to participate in theta synchronization of the medial septum. Here, we tested the hypothesis that HCN channel expression correlates with theta modulated firing behaviour of MS neurons by a combined anatomical and electrophysiological approach. HCN-expressing neurons represented a subpopulation of GABAergic cells in the MS partly overlapping with parvalbumin (PV)-containing neurons. Rhythmic firing in the theta frequency range was characteristic of all HCN-expressing neurons. In contrast, only a minority of HCN-negative cells displayed theta related activity. All HCN cells had tight phase coupling to hippocampal theta waves. As a group, PV-expressing HCN neurons had a marked bimodal phase distribution, whereas PV-immunonegative HCN neurons did not show group-level phase preference despite significant individual phase coupling. Microiontophoretic blockade of HCN channels resulted in the reduction of discharge frequency, but theta rhythmic firing was perturbed only in a few cases. Our data imply that HCN-expressing GABAergic neurons provide rhythmic drive in all phases of the hippocampal theta activity. In most MS theta cells rhythm genesis is apparently determined by interactions at the level of the network rather than by the pacemaking property of HCN channels alone.

(Received 15 April 2008; accepted after revision 17 June 2008; first published online 19 June 2008)
Corresponding author V. Varga: Department of Cell and Network Neurobiology, Institute of Experimental Medicine of the Hungarian Academy of Sciences; Szigony u. 43. Budapest, 1083 Hungary. Email: viktu@koki.hu

Hippocampal theta rhythm is a highly regular field potential oscillation coupled to information encoding during exploratory behaviours and REM sleep (Buzsaki, 2002). A GABAergic pathway running from the medial septum (MS) to the hippocampus plays a critical role in synchronizing the hippocampal neuron network at theta frequency (Freund & Antal, 1988; Toth *et al.* 1997). Remarkably, a large proportion of MS neurons fire in spike clusters called theta bursts tightly phase-locked to the ongoing hippocampal theta (Serafin *et al.* 1996). The elimination of GABAergic neurons in the MS abolished theta oscillation in the hippocampus (Gerashchenko *et al.* 2001; Yoder & Pang, 2005) and led to serious memory impairment (Dwyer *et al.* 2007). The recent advance of single cell labelling techniques enabled the identification of some major groups of theta burst firing neurons (TBN) in the MS showing that the majority of these cells are GABAergic and a subpopulation contains parvalbumin (Simon *et al.* 2006). Further investigations uncovered that parvalbumin-containing TBNs exhibit robust bimodal phase preference relative to hippocampal theta rhythm (Borhegyi *et al.* 2004). Altogether, these data raised the possibility that GABAergic TBNs or a subgroup of them can form a pacemaker population in the neuron network of the MS sending theta rhythmic input to the hippocampus.

Pacemaker cells in various tissues and in several brain regions express a non-selective cation channel family named hyperpolarization-activated and cyclic nucleotide-gated non-selective cation channels (HCN; Luthi & McCormick, 1998*a*). The block of HCN channels attenuates pacemaker activity in several cell-autonomously rhythmic neuron types (for review

This paper has online supplemental material.

 DOI: 10.1113/jphysiol.2008.155242

see Robinson & Siegelbaum, 2003). HCN expression was demonstrated in the MS of both rats and mice by *in vitro* electrophysiological and anatomical methods (Sotty *et al.* 2003; Morris *et al.* 2004). The presence of the HCN-mediated h-current was detected in fast spiking GABAergic and to a lesser extent in cluster firing glutamatergic neurons (Sotty *et al.* 2003). Furthermore, it was shown that HCN blockade in the MS of both anaesthetized and freely moving rats severely interferes with hippocampal theta-genesis manifested as a downward shift of theta frequency and reduction of regularity (Kocsis & Li, 2004). Despite the above detailed efforts the possible role of MS HCN-expressing neurons in theta rhythm generation is unknown.

Here, we aimed to unravel how HCN channels can contribute to the formation of theta oscillation in the MS by identifying and characterizing the neurons which express HCN channels utilizing combined *in vivo* electrophysiological, micropharmacological and anatomical methods. HCN-expressing neurons were found to form a subpopulation of MS GABAergic cells exhibiting regular, theta-rhythmic firing. We could also demonstrate that the HCN-positive cell group is heterogeneous based on the level of HCN expression, parvalbumin content, extent of theta modulation and relationship to hippocampal activity states. Furthermore, HCN was shown to influence the discharge frequency of HCN-expressing neurons.

Methods

Animal handling

In this study male Wistar rats weighing 200–400 g were used ($n = 299$, Charles River Kft., Budapest, Hungary or bred in the dedicated SPF animal facility of the Institute). Experiments were performed according to the guidelines of the Institutional Ethical Codex and the Hungarian Act of Animal Care and Experimentation (1998, XXVIII, section 243/1998), which conforms to the regulation of animal experiments by the European Union. Animals were kept under a 12 h–12 h light–dark cycle, and water and food were available *ad libitum*. All efforts were made to minimize pain and suffering and to reduce the number of animals used.

Anatomy

Retrograde tracing, and immunocytochemistry. To investigate the projection of HCN1/HCN2 neurons, five rats were used. Rats were anaesthetized with Equithesin (chlornembutal, 0.3 ml per 100 g), then placed in a stereotaxic apparatus. One hole had been drilled over one of the dorsal hippocampi, then the dura was removed and any debris or blood was cleared away from the brain surface. Septo-hippocampal cells were retrogradely labelled with green microsphere (Invitrogen–Molecular Probes, Carlsbad, CA, USA) injected by pressure through glass capillaries into the hippocampus at the following coordinates (Paxinos & Watson, 1998): 3.6 mm posterior to the bregma, 2 mm lateral to the sagittal sinus, and 2.4 mm vertically below the pial surface. Following injections, the capillaries were left in place for 15 min prior to removal to prevent the spread of the tracer back along the capillary track. After the injection procedure the wound over the calvaria was closed by polyamide monofilament suture (Dafilon; B. Braun/Aesculap AG, Tuttlingen, Germany) and the wound was treated by a mercury-containing antiseptic powder (Dermaforine, Pannonpharma Kft., Pécs, Hungary). Additional antibiotics were not given. The operated animals spent the 1 week survival time in a separated recovery room of our animal facility under daily supervision. It should be noted that all of the operated animals survived and recovered during the week-long survival period.

After 7 days survival time the rats with tracer injection, and five additional rats for the colocalization studies were anaesthetized with Equithesin and perfused through the heart first with physiological saline (1 min) and then with a fixative containing 0.05% glutaraldehyde, 4% paraformaldehyde, and 0.2% picric acid in 0.1 M phosphate buffer (PB; pH 7.4). For the *in situ* hybridization experiment, three additional rats were perfused with 4% paraformaldehyde under RNAase free conditions (diethyl pyrocarbonate (DEPC, Sigma-Aldrich Kft. Budapest, Hungary) was dissolved in solutions: see the *in situ* hybridization part of Methods for details).

Brains were removed and postfixed in glutaraldehyde-free fixative for 30 min to 2 h. Coronal sections of 80 μm thickness were cut on a vibrating microtome from tissue blocks of the injection sites, and 50 μm-thick sections were cut from the blocks of target areas, or for immunocytochemistry. For *in situ* hybridization the sections were processed first for GAD67 labelling (see below) followed by immunocytochemistry. The immunocytochemical procedures are as follows: sections were washed in 0.1 M PB, cryoprotected overnight in 30% sucrose dissolved in 0.1 M PB, and freeze-thawed in aluminium foil boats over liquid nitrogen to enhance penetration of the antisera. Next, after several changes of PB, the sections were transferred into Tris-buffered saline (TBS; pH 7.4). All the following washes and antisera dilutions were carried out in TBS. Sections were incubated in solutions of primary antibodies (guinea pig anti-HCN1 and 2, dilution: 1 : 500 (Notomi & Shigemoto, 2004); mouse anti-parvalbumin dilution: 1 : 1000, Swant) for 2 days. After the primary antisera were washed out, the following biotinylated secondary antisera were used for 2 hours: Alexa350 conjugated goat anti-mouse (1 : 50, Invitrogen–Molecular Probes) or FITC conjugated donkey anti-guinea pig or Alexa594 goat anti-guinea pig

(1 : 200, Invitrogen–Molecular Probes). After washing out of the secondary antisera the fluorescent labelled sections (immunoreaction and retrograde) were mounted in Aqua poly/mount (Polysciences Inc., Warrington, PA, USA). For light microscopy (HCN1–HCN2 colocalization) and electron microscopy biotinylated goat anti-guinea pig antisera (1 : 200, Vector Laboratories, Burlingame, CA, USA) were used for 2 h. Then, the sections were incubated in a solution of avidin-biotinylated horseradish peroxidase complex (ABC Elite; 1 : 200; Vector) for 2 h, followed by 3,3-diaminobenzidine 4HCl (DAB; Sigma-Aldrich) reaction (brown reaction product).

For colocalization and resectioning for electron microscopy the sections were embedded as follows: They were treated with osmium tetroxide (1% OsO_4 in 0.1 M PB for 1 h), then dehydrated in an ascending ethanol series (1% uranyl acetate was included in the 70% ethanol step for 40 min) and propylene oxide, and embedded in Durcupan resin (ACM, Fluka). The coexistence of two different antigens in the same cells was analysed by means of the mirror technique described by Kosaka *et al.* (1985). Briefly, immunoreactive perikarya cut in half at the surface of the sections, as well as nearby capillaries, were drawn with the aid of a camera lucida. The other halves of the immunoreactive somata were located on the matching surface of the adjacent section (incubated for the other antigen) by using the capillaries as landmarks.

To reveal the subcellular distribution of HCN immunoreactivity by electron microscopy 60 nm ultrathin sections were cut by a Leica Ultracut S or EM UC6 ultramicrotome (Leitz Microsystems GmbH, Wetzlar, Germany) and examined using a Hitachi H-7100 electron microscope (Hitachi, Ltd, Tokyo, Japan) equipped with a CCD camera (MegaView II, Olympus Soft Imaging Solutions GmbH, Münster, Germany).

Synthesis of riboprobes for GAD67

A segment of the rat GAD67 coding sequence (GenBank accession number: gi:204227, 764 bp from 773 to 1536) was amplified by RT-PCR from cDNA derived from Wistar rat hippocampal total mRNA sample (forward primer 5′- ATT GGT TTA GCT GGC GAA TG, reverse primer 5′- GCC TTG TCC CCT GTA TCG TA). The primers were designed using the Primer3 software (Rozen & Skaletsky, 2000). The PCR product was cloned into the *Sma*I site of pBluescript II SK$^-$ (Fermentas UAB, Lithuania). The integrity and orientation of the clone was verified by sequencing. GAD67 probe was linearized by *Hin*cII and *Xba*I digestion for the antisense and sense probe, respectively. The linearized template DNA was gel-extracted, precipitated, resuspended in diethylpyrocarbonate (DEPC)-treated H_2O at a concentration of 1 μg μl^{-1}, and stored at −20°C. *In vitro* transcription was carried out for 2 h at 37°C in a total volume of 20 μl containing 1 μg of template DNA, 1 × transcription buffer, 1 × DIG RNA Labelling Mixture, 40 units RNase Inhibitor and 20 units of T3 or T7 RNA polymerase, which was adjusted to 20 μl using DEPC-free double-distilled H_2O. All components were from Roche Molecular Diagnostics (Penzberg, Germany). Labelled riboprobes were DNase treated and purified using the RNeasy MinElute Cleanup Kit (Qiagen GmbH, Hilden, Germany). Finally, the integrity and quantity of the riboprobes were determined using gel electrophoresis.

In situ hybridization

All solutions used for *in situ* hybridization were first treated with 0.1% DEPC for 1 h and then autoclaved. Chemicals were purchased from Sigma-Aldrich Kft (Budapest, Hungary) unless otherwise indicated. Incubation of the 40 μm-thick rat brain slices was carried out in a free-floating manner in RNase-free sterile culture wells for all steps. First, the sections were washed in phosphate-buffered saline (PBST, containing in mM: NaCl, 137; KCl, 2.7; Na_2HPO_4, 10; KH_2PO_4, 2; and 0.1% Tween-20, pH 7.4) three times for 20 min. Hybridization was then carried out overnight at 65°C in 0.6 ml of hybridization buffer containing the digoxigenin-labelled riboprobe (0.7 μg ml^{-1}). Hybridization buffer consisted of 50% formamide, 5 × SSC, 1% sodium dodecyl sulphate (SDS), 50 μg ml^{-1} yeast tRNA and 50 μg ml^{-1} heparin in DEPC-treated H_2O. During the overnight incubation and the following three washing steps, the sections were continuously incubated on a shaker within a humid chamber. After incubation, the sections were first washed for 30 min at 65°C in Wash Solution 1 (containing 50% formamide, 5 × SSC, 1% SDS in DEPC-treated H_2O) and then twice for 45 min at 65°C in Wash Solution 2 (containing 50% formamide, 2 × SSC in DEPC-treated H_2O). The sections were next washed for 5 min in 0.05 M Tris-buffered saline containing 0.1% Tween-20 (TBST), pH 7.6 and then blocked in TBST containing 10% normal goat serum (TBSTN) for 1 h, both at room temperature. Next, sections were incubated overnight at 4°C with sheep anti-digoxigenin F_{ab} fragment conjugated to alkaline phosphatase (Roche Molecular Diagnostics) diluted at 1 : 1000 in TBSTN. The next day, the sections were washed three times for 20 min in TBST, and then developed with freshly prepared chromogen solution in a total volume of 10 ml, containing 3.5 μl 5-bromo-4-chloro-3-indolyl-phosphate and 3.5 μl nitro blue tetrazolium chloride dissolved in chromogen buffer (containing in mM: NaCl, 100; Tris-Cl, 100, pH 9.5; $MgCl_2$, 50; (–)tetramisole hydrochloride, 2; and 0.1% Tween-20). The sections were gently rinsed in 1 ml of the above developing solution in the dark for 7 h and the reaction

was stopped using PBST. Finally, the sections were washed in 0.1 M PB three times for 10 min, and were processed for immunohistochemistry.

Identification of juxtacellularly labelled neurons

During these experiments the postlabelling survival time had to be limited to increase the number of recovered and identified cells, thus compromising the completeness of their labelling. After the electrophysiological recording, labelling, and a short survival period (10–30 min), the animals were perfused transcardially, their brains were removed, and the block containing the medial septum was cut and postfixed overnight in glutaraldehyde-free fixative solution. Then, 60 μm sections were cut and treated as described above for the immunocytochemical experiments. The sections were incubated with streptavidin-conjugated Alexa 488 (1 : 3000; Molecular Probes) for 2 h to identify the biocytin (Sigma-Aldrich) or Neurobiotin (Vector Laboratories)-labelled neuron by fluorescent microscopy (Axioscope; Zeiss, Oberkochen, Germany). The wavelength for filter sets was as follows (absorption/emission in nm): 365 bandpass/420–460; 450–490/512–542; $546 \pm 12/590$ long pass. The section containing the labelled cell was immunostained for parvalbumin or HCN as described above, except that in this case the sections were incubated in primary antibodies overnight at room temperature. The results were documented by digital camera (DP-70; Olympus Optical, Tokyo, Japan), and the processing steps from here were similar to those described above for light microscopy (ABC and DAB).

The digitized images taken by the fluorescence or light microscope and the scanned electron microscopic negatives were further processed by Adobe Photoshop CS2 (Adobe Systems, San Jose, CA, USA).

Reconstruction of neurons was carried out by using the Neurolucida system (Microbrightfields, Williston, VT, USA).

Electrophysiology and pharmacology

Electrophysiological recordings and iontophoresis. Rats were anaesthetized by intraperitoneally injected 20% urethane solution at a dose of 0.7 ml $(100\ \mathrm{g})^{-1}$ (0.14 g $(100\ \mathrm{g})^{-1}$). A homeothermic heating pad connected to a rectal probe maintained the body temperature at $\sim$36°C (Harvard Apparatus, Holliston, MA, USA). A small window was drilled over the medial septum (AP: +0.3; L: +1.3; V: −4.5 to 6.5) and a hole over the right hippocampus (AP: −4.0; L: −2.5; V: −1.9 to 2.1). Electroencephalogram (EEG) from the hippocampus was recorded by a monopolar tungsten electrode (*in vitro* impedance = 0.8–3 MΩ; FHC, Bowdoinham, ME, USA) lowered into the pyramidal layer of the CA1 region using a mechanical microdrive (Hugo Sachs Electronic GmbH, Germany). During descent multiunit activity was monitored and an abrupt increase of the background noise with the occasional appearance of spikes around 1.9–2.0 mm from the brain surface marked the pyramidal layer. EEG was filtered between 0.3 Hz and 2 or 5 kHz, amplified at a ×5000 gain (BioAmp, Supertech, Pécs, Hungary), and digitized at 8.33 or 10 kHz by a CED micro1401 mkII system controlled by the Spike2 data acquisition software (CED, Cambridge, UK). Single units in the medial septum were recorded by glass microelectrodes pulled from borosilicate glass capillary (Sutter Instrument Co., Novato, CA, USA or WPI Inc. Sarasota, Fl, USA; 1.5 o.d., 0.75 or 0.86 i.d.) by a Flaming–Brown horizontal puller (P-87, Sutter). The tip of the electrodes was broken back if necessary to get a target impedance of 20–40 MΩ corresponding to 0.5–1.5 μm tip diameter. The electrodes were filled with 0.5 M NaCl containing 2% neurobiotin (Vector Laboratories). Positioning of the electrode was accomplished by a piezoelectric microdrive (Burleigh 6000 ULN or ISS 8200, EXFO, Quebec City, Quebec, Canada). The electrode descended along a tilted trajectory with deviation from vertical with an angle of 15 deg or 20 deg. Unit signals were amplified by a DC amplifier in bridge mode (Axoclamp 2B, Axon Instruments/Molecular Devices, Sunnyvale, CA, USA) and fed into a signal conditioner (LinearAmp, Supertech) for filtering (bandpass: 100 Hz and 5 kHz) and further amplification (final gain = 1000). The unit signal was digitized at 10 or 16.67 kHz using the same CED system as that used for the conversion of the EEG.

For iontophoresis the same type of electrode as that used for single unit recording was broken back to a tip diameter of $\sim$3–5 μm and glued to a flat piece of glass along with the single unit recording electrode in an angled position (for illustration see online supplemental material, Supplementary Fig. 2) by a glass bond (Loctite Ltd, Dublin, Ireland) under a light microscope. Tip separation was a maximum of 30 μm along each coordinate. For iontophoretic current injection the second channel of the DC amplifier was used. To eject drug a positive current of 20–50 nA was switched onto the iontophoresis electrode whereas a 5–10 nA negative holding current was applied to prevent the diffusion of the drug. Duration of current injection was 300–1400 s (see Supplemental material for details). Before drug application, control recordings of 120–300 min length were accomplished. During the course of drug injection, 30 s long sensory stimulation (tail pinch) was applied to induce theta at the following time points after the onset of ejection: 60, 180, 300, 600, 900 and 1200 s. In some cases the onset of sensory stimulation could vary.

Since ZD7288 has not been applied *in vivo* by utilizing iontophoresis prior to the start of our iontophoresis measurements, we carried out control recordings in

slice preparations to tune the parameters of the *in vivo* experiments. The final parameters were verified *a posteriori* by an independent study (Wang *et al.* 2007). Further details on iontophoresis are presented as Supplemental material.

Electrophysiological experiments were concluded in two ways: in the case of successful juxtacellular labelling, rats were left in place for a short survival period (maximum 1 h) and then transcardially perfused (see the corresponding part of the Methods: Identification of juxtacellularly labelled neurons). If the recorded neuron could not be labelled the animal was overanaesthetized by a high dose of urethane (double or triple of the normal 0.14 g/100 g dose) delivered intraperitoneally.

Drugs and doses used for iontophoresis

All drugs were dissolved in distilled water and pH was set to ∼8–9, and thus the applied drugs were ejected as cations. Concentrations were as follows: bicuculline methiodide (Sigma-Aldrich) in 2 or 10 mM, ZD7288 (Tocris Biosciences, Bristol, UK) in 0.5 or 5 mM.

Data analysis

Selection of EEG segments. First, based on the time–frequency analysis of the EEG, theta and non-theta segments were separated as described earlier (Borhegyi *et al.* 2004). Briefly, the EEG was subjected to continuous wavelet transformation following down-sampling to 200 Hz as previously described. As the wavelet base function, the Morlet wavelet was chosen. To calculate the wavelet transformation, the algorithm of Christopher Torrence was used (Torrence & Compo, 1998). Further details about the applied wavelet transform can be found in the previous reference.

Based on wavelet amplitude values, the ratio between signal power in the 2.5–6 Hz and 0.5–2.5 Hz ranges was calculated (∼ theta/delta ratio or TDR) for each data point and then the mean and standard deviation of these values were determined. Theta segments were defined as parts of the EEG with TDR higher than the mean + 0.5 S.D. Non-theta segments were defined as periods with power maxima of the wavelet falling outside the theta band. From the theta episodes, those elicited by tail pinch were used for further analysis as these were longer and more regular, and the septo-hippocampal phase coupling (in the case of theta bursting MS neurons) was tighter than that observed during spontaneous episodes. From the non-theta segments those with a length of > 5 s and without the occurrence of ripple events were used (except 4 recordings, in which a maximum of 2 ripples occurred in the analysed non-theta segments). Ripples were selected in the following way (Klausberger *et al.* 2003): first, the EEG was digitally filtered between 95 and 145 Hz using the built-in FIR filter of Matlab (The Mathworks Inc., Natick, MA, USA) with an order of 512 and the filtfilt function, which enables filtering without introducing a phase shift. Then, the root mean square (r.m.s.) of the signal was calculated in 10 ms windows and ripples were defined as events with peak amplitude larger than the mean + 5 S.D. of the r.m.s. of the signal. The points around the ripple peaks at which the r.m.s. function intersected a mean + 1 S.D. threshold were defined as the beginning and end of ripples. The firing activity of MS units during ripples was determined by calculating the spike count during ripples. Ripple-associated activation or inhibition was defined as a $> 50\%$ increased or reduced firing rate during ripples compared to that during non-theta (no ripple). Additionally, peri-event time histograms were constructed centred at ripple peaks by using ± 250 ms time lag and 10 ms bin size.

General firing parameters and characterization of theta-modulated firing. Before the analysis spikes were amplitude-discriminated. The amplitude-discriminated unit signal was converted into a vector containing 0s between spikes and 1s in place of spikes. Then, the firing rate and theta modulation were determined. The latter was defined as the proportion of power in the theta band of the autospectrum of the unit signal, also called relative theta power. The autospectrum was calculated by generating the power spectral density estimate of the autocorrelation function using the Welch method as implemented in the pwelch function of Matlab. The resolution of the spectral estimate was 0.2 Hz. Ten millisecond bins were applied for the calculation of the autocorrelograms and only the central 512 points (0 + 512) of the autocorrelogram were used in the spectral calculations. Theta modulated firing was also analysed in the time domain by introducing a measure called the theta propensity index (TPI) utilizing the high time resolution of the wavelet transform. TPI was determined as follows: the 0–1 vector derived from the spike train was convoluted with a sinc function and down-sampled to 200 Hz. For the wavelet calculation the same parameters were used as introduced for the transform of the EEG. After generating the wavelet, the amplitude maxima at each time point were selected and the corresponding frequencies were determined (Roux *et al.* 2007). This frequency vector was calculated for the EEG-wavelet as well. From the two frequency vectors the following ratio was calculated: time during which the unit was in the theta band/time while the EEG was in theta band. This ratio was named the theta propensity index. It is important to emphasize that for this calculation the entire recording segment was used in each neuron. A value < 1 shows that the unit was weakly theta modulated (non-bursting or tonic cells), ∼1 that the theta bursting of the unit was strictly coupled to the theta rhythm in

the EEG (tail pinch responsive cells), > 1 that the unit fired during both EEG theta and non-theta episodes (strongly theta-modulated, non-theta-associated theta bursting or constitutive bursting cells). The procedure of TPI calculation is also explained in Supplementary Fig. 1. TPI value was analysed with the burstiness index expressing the propensity of firing in theta burst mode (see the next section).

Analysis of theta bursts. To further analyse the firing pattern of MS neurons, spike clusters occurring at theta frequency and having higher intracluster than intercluster frequency (named theta bursts) were separated by using a joint tree clustering method (Borhegyi *et al.* 2004). Briefly, interspike intervals were subjected to the cluster analysis using Euclidean distance and Ward's amalgamation rule. Intervals belonging to the selected theta and non-theta segments were analysed separately. The icicle plot (dendrogram) was cut at various linkage distances to generate two to seven clusters. After each cut the cluster containing the largest number of interspike intervals was selected as the potential burst cluster assuming that the majority of intervals occur within theta bursts when the neuron fires in theta burst mode. The interval distribution of the six selected burst clusters was plotted and visually compared to the distribution of all interspike intervals (ISIH) of the analysed segment. As theta bursting neurons have a characteristic bimodal interspike interval distribution, the cluster producing an interval distribution which overlaps with the first peak of the ISIH was selected. Finally, the bursts were marked on the train for *post hoc* verification. The following burst parameters were calculated: (i) burtiness index (BI) = proportion of intervals in theta bursts; (ii) frequency of burst occurrence (= the reciprocal of the intervals between the first spikes of bursts); (iii) number of spikes in theta bursts (intraburst spike number: IBSN); and (iv) length of theta bursts (BL); *versus* average instantenous frequency within theta bursts.

Analysis of phase preference. The phase relationship of MS unit activity and hippocampal EEG was determined by calculating the instantaneous phase difference of the two signals based on cross-wavelet phase values (Borhegyi *et al.* 2004; Li *et al.* 2007). The argument of cross-wavelet coefficients corresponds to the instantenous phase difference values. Cross-wavelet amplitude maxima falling into the theta band were selected and sorted in ascending order. Phase was extracted from wavelet coefficients corresponding to the upper quartile of the sorted amplitude values. Thus, phase difference was obtained for data points when coupling strength surpassed 75% of maximum. The resulting phase angles were further analysed by circular statistics (Fisher, 1993). For each neuron the phase histogram was determined and tested against the null-hypothesis of uniformity by Rao's spacing test and Watson's test for uniformity. Then, the circular mean, standard deviation, variance and mean vector length were determined, the last analogous to coupling strength. To test whether the identified anatomical classes show group-level phase preference, a cumulative phase histogram of each anatomical group was generated. To this end from the cross-wavelet phase values of each neuron 5000 were selected based on the corresponding coupling strength. These values were pooled for each anatomical class and subjected to the same tests as phase values of individual neurons. In case of the double immunoreactive HCN/PV group the distribution of phase angles was bimodal, which was verified by fitting the distribution with the mixture of two von Mises probability density functions. The mixing ratio, error of estimate, mean angles and concentration parameters (κ) belong to the peaks were calculated. The phase distributions of anatomical classes were compared using Watson's test.

Analysis of iontophoresis data. The effect of the administered drugs was quantified by determining the same parameters for the drug application period as those for control recordings except the theta propensity index, which was omitted from this part of the analysis. Theta and non-theta periods were analysed separately and basic firing parameters (firing rate and theta modulation) were calculated in 5.5 s non-overlapping windows. In the statistical comparison of subsequent time periods, segments containing a minimum of three windows were compared. When calculating the onset of significant drug action, the beginnings of segments being significantly different from control, pre-drug periods were given. Additionally, in order to test whether the iontophoresis of ZD7288 has any effect on theta activity in the hippocampus, the frequency and power of 20 s-long segments of tail pinch-induced theta episodes of the hippocampal EEG during control and drug application periods were also calculated and compared using Friedman's ANOVA.

All of the above analyses were accomplished by using self-devised scripts in the Matlab environment.

Data presentation and statistical tests. As the distribution of the analysed parameters deviated from normal in most cases the median values were presented throughout in the text of Results and also in tables (except phase data). All pairwise comparisons (except in the case of circular data) were done by Mann–Whitney U test. Dependence of firing pattern/firing rate and HCN immunoreactivity was tested by χ^2-test. Anatomical group and physiological parameter interactions were further investigated using repeated

measures ANOVA with anatomical identity as the grouping variable and hippocampal state (non-theta, theta, ripple) as the repeated measures factor. In the iontophoresis experiments drug–time interactions were tested by repeated measures ANOVA using dose as the grouping variable and postinjection time as the repeated measures factor. The effect of drugs on firing parameters were also tested in each neuron by comparing the consecutive time segments or the stimulation-elicited theta periods by Friedman's ANOVA (multiple comparisons) the sign test or the Wilcoxon matched-pairs test (pair-wise comparisons). Threshold of significance was set to 0.05. The statistical tests were carried out using Statistica (Statsoft Inc., Tulsa, OK, USA).

Results

HCN immunoreactivity is abundant in the medial septum and localized mostly to soma-dendritic membranes

In order to analyse the possible roles of HCN channels in the medial septal network, their distribution was examined by light and electron microscopy. Pacemaker subunits HCN1 and HCN2 are expressed throughout the medial septum, in the area surrounded by cholinergic cells forming a non-overlapping population with the latter cell group. Immunoreactivity for both subunits was observed on soma-dendritic membranes, in thick, proximal dendrites, in distal, small diameter dendritic profiles and to a lesser extent in small puncta, indicative of axon varicosities (Fig. 1*A*). In some cases cytoplasmic staining was also detected. Besides the HCN1 subunit, the distribution of HCN2 and their colocalization was also examined. By using Kosaka's mirror technique (Fig. 1*G* and *H*) the two subunits showed virtually full colocalization in neuronal profiles. In several cases (as can be seen in Fig. 1*H* marked by arrowheads), labelling of oligodendroglia by the HCN2 staining was also observed (Notomi & Shigemoto, 2004).

At high magnification, a large variability in HCN1 staining pattern was observed. Neurons were outlined by strong HCN1 labelling evenly along the plasma membrane, whereas faint punctate signals visualizing only small HCN1-positive dots were also found. To reveal whether the variability in labelling arose from different levels of surface HCN expression, or the weak, punctate signal indicated other subcellular domains, for example axon terminals surrounding an immunonegative cell body, the subcellular localization of HCN1 channel was further investigated by electron microscopy (Fig. 2). Regions containing immunoreactive elements with different labelling pattern were reembedded, and ultrathin sections were cut and examined. As with light microscopy, large variability in plasma membrane staining was found. Soma-dendritic membranes were evenly covered with reaction product, whereas in other cases islet-like, intermittent concentration of staining, surrounded by immunonegative membrane segments, was observed (Fig. 2*A*–*C*, on *B* see arrows). Only very few immunoreactive terminals were found. The analysis of a total of 2208 μm perimeter membrane uncovered that HCN1-immunoreactive boutons did not establish synaptic contacts on HCN1-positive soma-dendritic membranes (for an HCN1-IR terminal contacting an HCN-immunonegative profile see Fig. 2*D*). Apart from intracellular membrane-associated signal in somata and dendrites, labelling was occasionally seen in myelinated axons.

HCN-immunoreactive neurons are GABAergic and a subpopulation contains parvalbumin

To determine whether HCN-expressing cells are indeed GABAergic, or whether cholinergic neurons can also express HCN, we carried out double staining experiments. Three markers, the 67 kDa isoform of the GABA-synthesizing enzyme glutamic acid decarboxylase (GAD67), the calcium-binding protein parvalbumin labelling septo-hippocampal GABAergic projection neurons, and the acetylcholine synthesizing enzyme choline-acetyl transferase (ChAT), were used, because these proteins are expressed by the two major neuron populations, the GABAergic and cholinergic cell groups of the MS (Kiss *et al.* 1990). Since most of the GAD protein is transported into the axon terminals resulting in low protein levels in neuronal somata of long projecting cells, the detection of GAD67 mRNA by *in situ* hybridization was preferred instead of immunocytochemistry. Thus, free-floating sections from three animals were first labelled by the GAD67 probe and then were processed for HCN1 immunofluorescence. Out of 113 unequivocally HCN1-immunoreactive neurons, all contained GAD67 mRNA demonstrating that these cells are indeed GABAergic (see Fig. 1*B* and *C*). In six additional cases the *in situ* hybridization signal was weak while in five other cases the intensity of the immunolabelling was too low. In the opposite direction, the proportion of HCN1-immunonegative neurons in all GAD67 expressing cells could not be conclusively shown because of weakness or lack of HCN1 signal that could have been caused by the *in situ* procedure. In agreement with the above results, all examined HCN1-IR neurons were found to be ChAT-immunonegative by double immunofluorescent labelling demonstrating that cholinergic MS neurons do not express HCN1. In light of the heterogeneous firing pattern of PV neurons documented in our previous study (Borhegyi *et al.* 2004), we examined (using HCN1/HCN2 and PV double immunolabelling) the colocalization between HCN1/2 and PV. Around the midline of the

medial septum (Fig. 1*A*), out of 486 immunolabelled cells, 21% of the PV-expressing neurons colocalized with 55.8% of HCN1-immunoreactive neurons.

The area in the medial septum occupied by HCN1/HCN2-IR neurons was found to be medial to the territory of the main cholinergic neuron population. Only a couple of cholinergic neurons (less than 5%, 3–6 neurons/50 μm sections) in the midline were located among HCN-IR neurons and therefore were checked for possible double ChAT/HCN1 or HCN2 immunolabelling. None of the examined ChAT-expressing neurons were immunoreactive for HCN1 or HCN2 (11 sections of 2 animals were analysed).

As medial septal GABAergic neurons project to various brain regions, we investigated whether the hippocampus is among the targets of HCN1 neurons (see Fig. 1*D–F*). Since all septo-hippocampal fibres cannot be labelled and the injection placement can heavily influence the number of back-filled cells, only qualitative analysis was done. Among retrogradely labelled neurons all types were observed: HCN1/PV double-immunoreactive, HCN-IR/non-PV, non-HCN/PV-IR and non-HCN/non-PV.

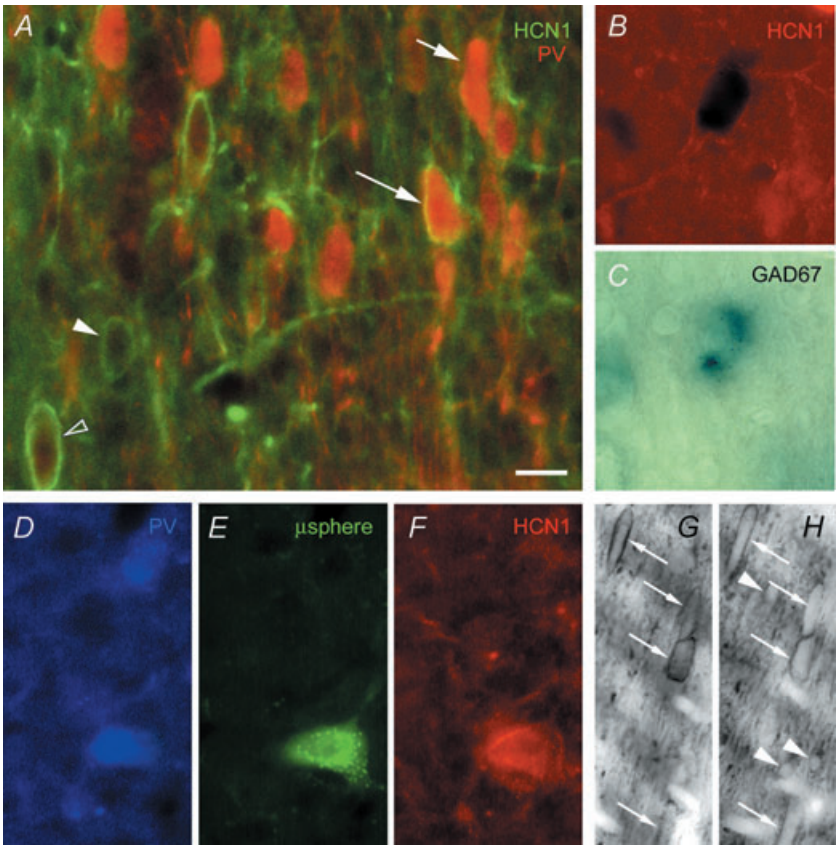

Figure 1. Colocalization of HCN1 immunoreactivity with neurochemical markers
A, double immunolabelling of HCN1 (green) and parvalbumin (red) is shown. The long arrow points to a double-labelled neuron while the short arrow indicates a non-HCN, PV-containing neuron. The filled arrowhead marks a single labelled HCN1-immunoreactive neuron. Note the different intensity of HCN1 labelling: the open arrowhead marks a strongly labelled, while the filled arrowhead points to a weakly stained, HCN1-immunoreactive neuron (see also Fig. 2). *B* and *C* represent the result of the GAD67 *in situ* HCN1 immunocytochemistry double labelling. Free-floating sections were labelled by the GAD67 probe (dark blue reaction product) and HCN1 immunocytochemistry. *B*, fluorescence photomicrograph presenting a double labelled neuron (note the shading effect of the *in situ* precipitate); *C*, the same cell on a light microscopic photomicrograph. *D–F*, retrograde labelling experiment, in which fluorescent microsphere was injected (green) into the hippocampus, and the medial septal sections containing the retrogradely labelled neurons were immunostained for parvalbumin and HCN1. *E*, a retrogradely labelled septo-hippocampal neuron double-stained for PV (*D*) as well as HCN1 (*F*) is shown. *G* and *H*, HCN1 and HCN2 stain the same cell population in the medial septum. In these panels representative sections used for examining the colocalization by Kosaka's mirror technique are demonstrated. Arrows point to labelled neurons: in *G* one half of each cell was stained by HCN1, in *H* the corresponding other half of the cells was labelled by antibody against HCN2. Arrowheads indicate the presence of oligodendrocytes in the HCN2 staining, since these cells do not express the HCN1 subunit. Scale 10 μm for *A–F*, 20 μm for *G* and *H*.

Physiological characterization of HCN-immunoreactive neurons

In the present experiments 37 medial septal neurons out of 99 labelled and recovered cells were identified as HCN1-immunoreactive (HCN-IR; $n = 25$) or HCN1-immunonegative (non-HCN, $n = 12$). Thirty-one neurons (22 HCN and 9 non-HCN) were also tested for parvalbumin (PV) immunoreactivity and 14 HCN-IR neurons were found to be immunopositive for PV as well. One HCN-immunonegative, PV-IR neuron was found. The firing pattern and its relationship to the two major hippocampal network patterns – theta rhythm and large amplitude irregular activity with sharp waves (LIA) – were analysed for all identified neurons. For the summary of the electrophysiological characteristics of the identified anatomical groups see Table 1. Representative examples of the anatomical groups are shown in Fig. 3 (immunocytochemical identification) and Figs 4 and 5 (state-dependent firing patterns of HCN-IR and non-HCN neurons, respectively).

The presence of theta rhythmicity is characteristic of the firing pattern of HCN-IR neurons

All HCN-IR neurons ($n = 25$) exhibited theta rhythmic activity accompanying the spontaneous or tail pinch-induced formation of theta oscillation in the hippocampus (Fig. 4*A*–*C*). In sharp contrast, only 4 of 12 non-HCN neurons showed theta rhythmic firing coupled to hippocampal theta activity (see Fig. 5*B*). One non-HCN neuron fired spike clusters at low, non-theta frequency (Fig. 5*C*) during hippocampal theta.

In order to quantify the difference between HCN-IR and non-HCN neurons in the theta-content of firing pattern, the proportion of power in the theta band of unit autospectra (i.e. relative theta power expressed in percentage) was calculated for non-theta and theta

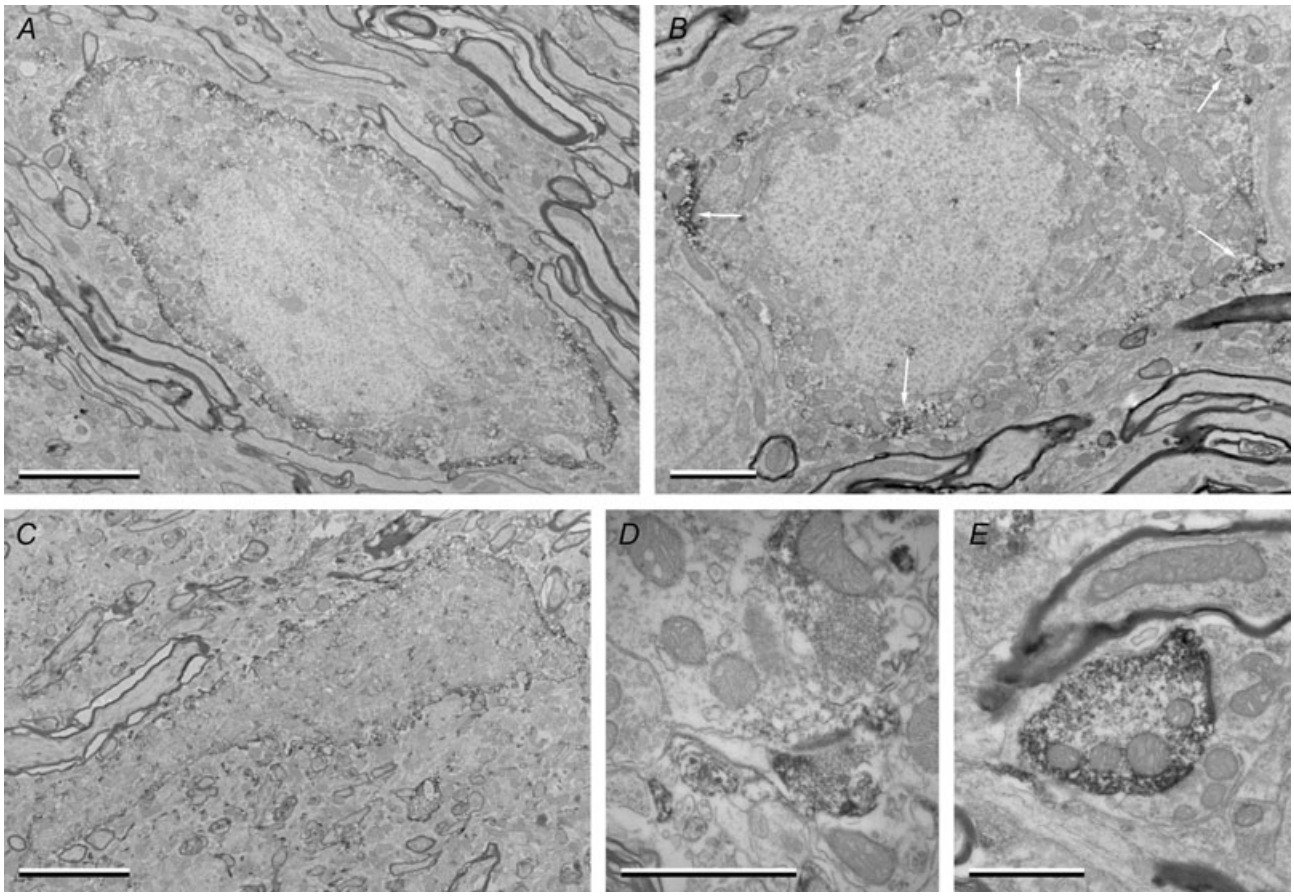

Figure 2. Subcellular localization of HCN1 subunits revealed variable intensity of labelling
The electron-dense DAB reaction product resulting from HCN1 immunoreaction can be observed in membranes of somata (*A* and *B*), dendrites (*C* and *E*) and infrequently in axons (*D*). The strength of soma labelling was highly variable ranging from strong, which continuously delineates the plasma membrane (*A*), to weak, patchy labelling indicating the uneven concentration of immunogenic material along the perimeter of the soma (*B*: arrows indicate few patches) supporting the light microscopic observation of variable expression levels of HCN ion channels on MS neurons. Scales: *A* and *C*: 5 μm; *B*: 2 μm; *D* and *E*: 1 μm;

Table 1. Electrophysiological characteristics of identified anatomical groups

	Firing rate (Hz)			Theta modulation (%)		TPI
Group	B	TP	R	B	TP	
All HCN ($n = 25$)	12.79 ± 8.71	19.25 ± 7.55	14.01 ± 14.54	10.47 ± 11.66	55.10 ± 35.85	1.31 ± 1.37
PV/HCN ($n = 14$)	12.02 ± 8.55	19.82 ± 6.15	14.57 ± 17.59	14.94 ± 22.09	57.07 ± 34.40	1.74 ± 2.29
Non-HCN ($n = 12$)	11.65 ± 11.79	15.15 ± 11.52	7.47 ± 9.11	3.93 ± 4.96	11.38 ± 31.05	0.58 ± 0.73

	Burstiness (%)		Intra-burst F (Hz)		Spikes in burst		Burst length (ms)	
	B	TP	B	TP	B	TP	B	TP
All HCN ($n = 11/24$)*								
Baseline bursting	95 ± 5	99 ± 4	36.9 ± 5.5	48.2 ± 22.7	5.1 ± 2.6	5.6 ± 3.4	108 ± 22.7	98.3 ± 21.2
All bursting	—	98 ± 3**	—	46.7 ± 25.8	—	5.6 ± 3.3	—	98.8 ± 39.3
PV/HCN ($n = 9/14$)*								
Baseline bursting	97 ± 5	99 ± 2	36.9 ± 11.2	44.6 ± 21.4	5.1 ± 1.6	5.6 ± 1.8	108 ± 22	98.3 ± 20.1
All bursting	—	99 ± 2**	—	46.7 ± 21.7	—	5.5 ± 2.9	—	95.9 ± 21.2
Non-HCN ($n = 0/4$)*	ND	0 ± 94**	—	30.9 ± 12.7	—	4.7 ± 2.1	—	114 ± 44.6

Values are median ± interquartile range; B: baseline = non-theta; TP: tail pinch = theta; R: ripple; TPI: Theta Propensity Index = duration of theta in unit/duration of theta in EEG calculated for the entire recording period of each neuron. All HCN: all HCN neurons were included (PV-IR, non-PV and those not tested for PV-content); PV/HCN: the PV-containing subgroup of all HCN cells; ND: not detected, e.g. in case of non-HCN neurons theta bursts were not observed during non-theta; *: in brackets the first number denotes neurons firing in theta bursts during non-theta periods whereas the second number equals to all theta bursting neurons in that category; **: for the calculation of burstiness during theta all bursting and nonbursting neurons thus, $n = 25$ HCN, $n = 14$ PV/HCN and $n = 12$ non-HCN were included.

segments. By using repeated measures ANOVA significant 'anatomical group'–'hippocampal state' interaction was revealed (groups: HCN *versus* non-HCN; states: non-theta *versus* theta; $P < 0.01$, $n = 37$). By pairwise comparison of HCN-IR and non-HCN neurons (all pairwise comparisons were carried out by Mann–Whitney U test; see also Methods), it was shown that relative theta power of the former group was significantly higher than that of the latter neurons during both the non-theta (median ± interquartile range: 10.47 ± 11.66% *versus* 3.93 ± 4.96%; $P < 0.01$, $n = 25$ HCN-IR *versus* 12 non-HCN), and theta periods (55.1 ± 35.85% *versus* 11.38 ± 31.05%; $P < 0.001$, $n = 25$ *versus* 12; see Table 1). The HCN-IR subgroups, i.e. PV-containing and PV-negative neurons, did not exhibit statistical difference in the extent of theta modulation during the analysed hippocampal EEG states (non-theta PV-IR *versus* non-PV: 14.94 ± 22.09% *versus* 6.89 ± 4.85%; theta PV-IR *versus* non-PV: 57.07 ± 34.4% *versus* 32.65 ± 28.63%; $P > 0.05$, $n = 14$ PV-IR *versus* 8 non-PV HCN neurons; note that 3 HCN-IR neurons were not tested for PV-IR, and were thus excluded from this comparison).

The firing pattern of the majority of HCN-IR neurons was dominated by theta rhythm independent of hippocampal states

The overall higher theta content of HCN-IR *versus* non-HCN neuronal firing pattern may result from the longer duration of theta rhythm in unit activity arising partly independently from the hippocampal EEG in the former group. Therefore, the total length of theta-dominated segments of unit activity was calculated and normalized by the duration of theta episodes in the hippocampal EEG (details of calculation are presented in Supplementary Fig. 1). The resulting parameter was called the theta propensity index (TPI). A value larger than 1 means that the cell fired in a theta-modulated manner for a longer time than theta was present in the hippocampal EEG. Fourteen of the 25 HCN-IR neurons (56%) were characterized by a TPI value > 1, whereas in the HCN-immunonegative neuron group only 2 out of 12 cells (16.7%) had a TPI value > 1. Accordingly, the TPI of HCN neurons (both PV-IR and PV-negative, subgroups were not significantly different and pooled) was significantly higher than that of non-HCN cells (1.31 ± 1.37 *versus* 0.58 ± 0.73; $P < 0.001$, $n = 25$ *versus* 12; see also Table 1).

Analysis of theta burst firing of HCN-IR and non-HCN neurons

Theta rhythmic neurons can fire multiple action potentials tightly coupled to hippocampal theta waves (Ford *et al.* 1989). These action potential groups were called theta bursts and were defined as statistically separable spike clusters occurring at theta frequency and characterized

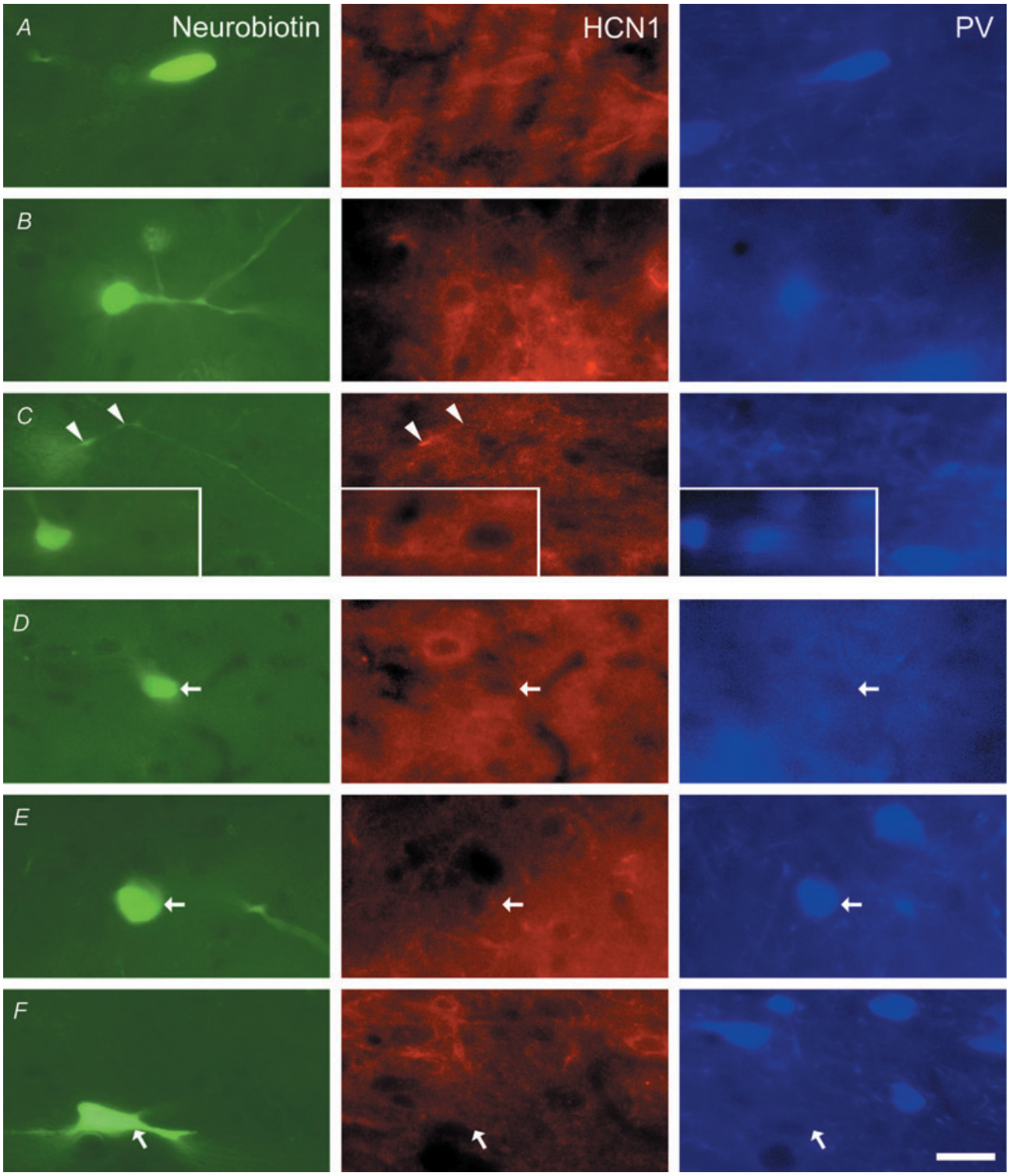

Figure 3. Immunocytochemical identification of HCN-IR and non-HCN neurons presented on Figs 4 and 5

Left column, the neurobiotin-labelled cell body and/or dendrites; middle column, HCN1 immunoreactivity; right column, PV staining. In *A–C* the representative examples of the electrophysiological categories of HCN-IR neurons of Fig. 4 are shown. Cells in panels *A* and *B* contain PV besides HCN1. Arrowheads on panel *C* mark an HCN1-immunoreactive dendritic trunk close to the section surface. In *D–F* three non-HCN cells shown on Fig. 5 are presented. The neuron in panel *E* was proved to be PV immunoreactive. Arrows point to the somata of HCN1-immunonegative cells. See also the HCN1-immunoreactive elements in the vicinity of the immunonegative neurons. Scale bar in the lowermost right corner = 20 μm.

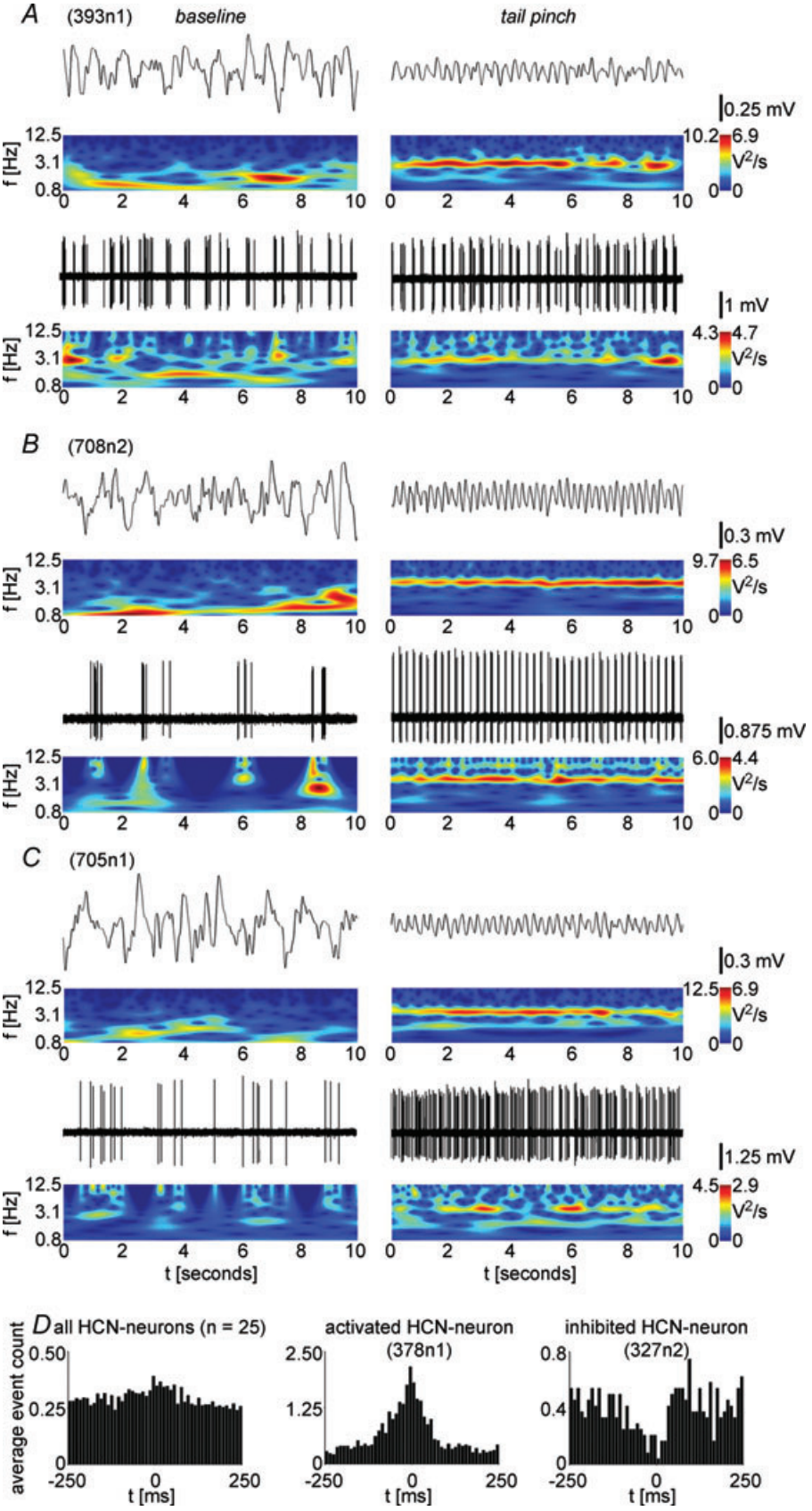

by high intracluster instantaneous frequency. Thus, we investigated whether theta-modulated HCN-expressing and non-HCN neurons exhibit theta burst firing pattern during hippocampal theta and/or non-theta states. A burstiness index (BI) was introduced that expresses the proportion of spikes in theta bursts relative to all spikes fired during the analysed periods (see also Methods). From the total of 25 HCN-IR neurons 24 (96%) fired in a theta bursting manner concurrently with hippocampal theta (Fig. 4*A* and *B*, right column). Eleven of these HCN-IR neurons exhibited theta bursting even during hippocampal non-theta states (Fig. 4*A* presents an example) whereas the remaining 13 HCN-IR neurons fired irregularly during non-theta periods (Fig. 4*B*, left column). In the case of the remaining single HCN-IR neuron, separable theta bursts could not be observed, but strong theta modulation was detected during both non-theta and theta segments (see Fig. 4*C*). Among HCN-immunonegative neurons only 4 out of 12 (25%) produced theta burst activity coupled to hippocampal theta (an example is presented on Fig. 5*B*). One non-HCN neuron fired spike clusters at half of the frequency of the ongoing hippocampal theta (Fig. 5*C*). In contrast to HCN-IR neurons, non-theta-associated theta bursting of HCN-negative neurons was not observed. Thus, the presence of HCN channels and theta burst firing pattern were proved to be highly significantly interdependent at $P < 0.0001$ by χ^2-test ($n = 37$). The connection between HCN immunoreactivity and theta burst firing was further supported by the significantly higher burstiness index of the HCN-IR neuron group compared to that of HCN-negative cells both during non-theta ($0 \pm 97\%$ *versus* $0 \pm 0\%$; $P < 0.001$, $n = 25$ *versus* 12) and theta states ($98 \pm 3.5\%$ *versus* $0 \pm 94\%$; $P < 0.001$, $n = 25$ *versus* 12; see also Table 1).

By comparing the characteristics of theta bursts of HCN-IR ($n = 24$) and non-HCN neurons ($n = 4$), the interspike intervals within the theta bursts of the former group were found to be shorter resulting in significantly higher average intraburst instantenous frequency than that observed in the case of non-HCN cells (46.7 ± 25.8 Hz *versus* 30.9 ± 12.7 Hz; $P < 0.05$; refer to Table 1 for the comparison of burst characteristics). Statistical difference in other burst parameters could not be detected.

As described earlier, 14 HCN-IR neurons were modulated at theta frequency during hippocampal non-theta states indicated by > 1 TPI value. From these cells 10 fired separable theta bursts (and one was only theta modulated). Four of these 10 HCN-IR neurons spent the entire length of the analysed non-theta period in theta bursting mode that was less regular than the rhythmic firing during hippocampal theta (in a previous study – Borhegyi *et al.* 2004 – these neurons were called constitutively bursting, see Fig. 4*A* for an example). By comparing non-theta- and theta-associated burst genesis, the induction of hippocampal theta was found to result in the significant acceleration of theta burst formation (from 2.77 ± 0.92 Hz during hippocampal non-theta to 3.43 ± 0.62 Hz coupled to theta; $P < 0.05$, $n = 11$, compare the non-theta- and theta-associated firing pattern of the cell in Fig. 4*A*).

In summary, firing pattern analysis of the recorded and identified neurons unraveled that regular, theta-rhythmic firing is a dominant attribute of the HCN-expressing group. While a small proportion of non-HCN neurons

Figure 4. Firing behaviour of HCN-IR neurons
Significant theta rhythmic component characterized all firing pattern types exhibited by HCN-IR neurons. Ten second long segments were selected from baseline (left column) and tail pinch-induced theta periods (right column). Under each raw data trace the corresponding wavelet spectrum (time–frequency decomposition) is shown. Theta band is in the upper half of the wavelet spectra (between 2.5 and 6 Hz). Warmer colours indicate higher magnitude (numbers on the left/right side of colour bars corresponds to the range of magnitudes of wavelet coefficients on left/right wavelet spectra). *A* demonstrates a representative example of neurons ($n = 11$, number in brackets is the code of the depicted neuron) firing in theta burst mode not only associated with hippocampal theta but occasionally during non-theta states as well. In the left column an episode of theta bursting can be observed while the hippocampal EEG is dominated by slow, non-theta activity. Note that spike clusters occurred at lower frequency and intercluster interval was more variable than during hippocampal theta-associated bursting (right column). The induction of theta changed the firing pattern of these neurons to more regular with tight phase coupling of bursts to hippocampal theta waves. The neuron in *B* fired irregularly paced spike clusters or single spikes during baseline segments whereas its activity was rendered to highly regular theta bursting in parallel with the formation of hippocampal theta ($n = 13$ HCN-IR neurons showed this type of firing behaviour). The only non-bursting HCN-IR neuron presented in *C* did not produce separable theta bursts despite the occasional theta modulation of its firing pattern (see the warm-coloured spots in the theta band of the lowermost wavelet spectrum in the right column). *D*, the ripple-associated firing activity of HCN-IR neurons. Peri-event time histograms centred at ripple peaks of all (left, $n = 25$), an activated (middle) and an inhibited HCN-IR neuron (right) are presented. The lack of a clearly separable peak on the group histogram (left) indicates that the ripple-associated activity change was not a distinguishing characteristic of the HCN-IR neuron group. However, the analysis of individual cells revealed diverse behaviours during ripples. Bin size of peri-event time histograms: 10 ms.

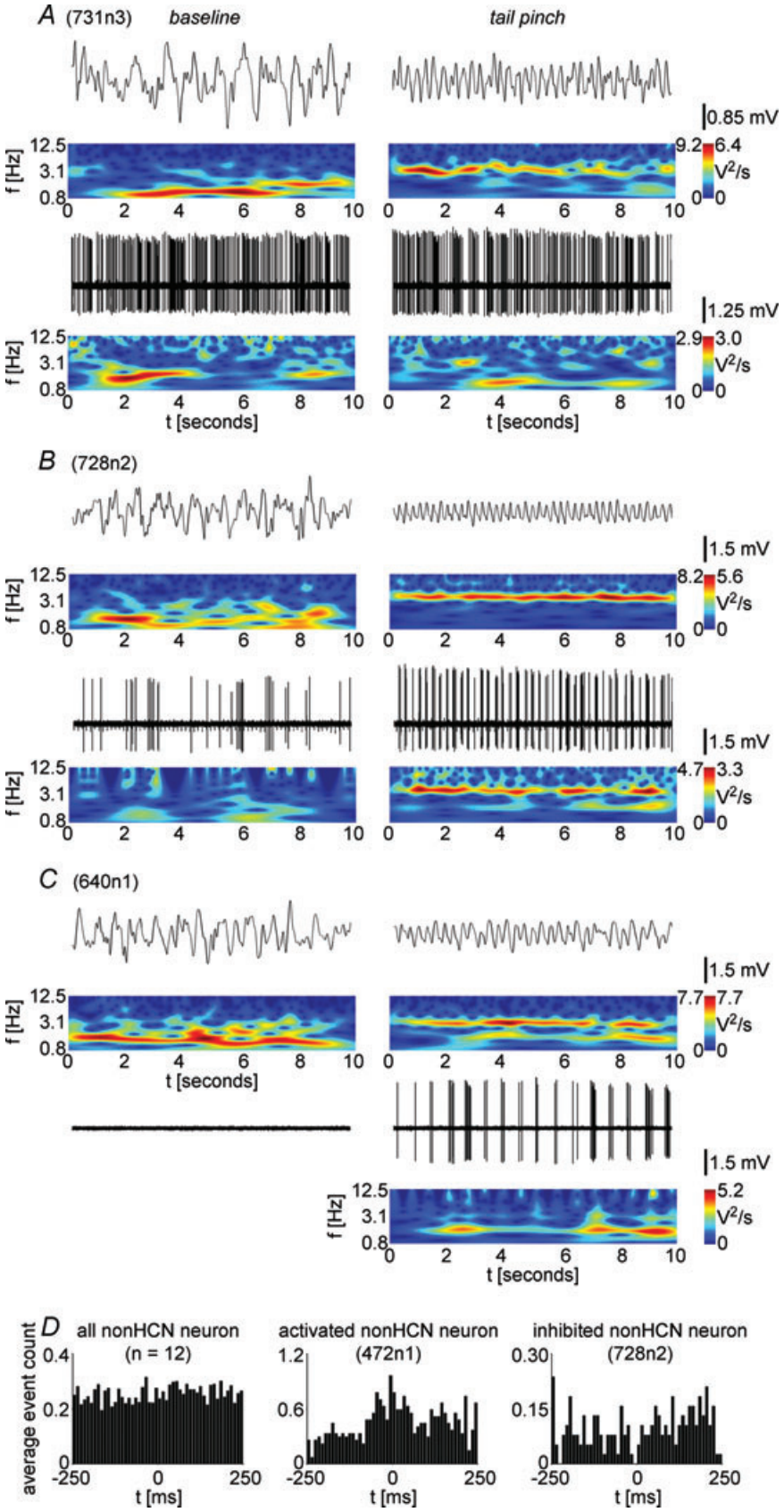

Figure 5. Firing behaviour of non-HCN neurons
The organization of the figure is the same as for Fig. 4. The neuron in *A* belongs to the most populous non-HCN neuron subgroup ($n = 7$): these cells fired irregularly during both baseline and theta periods not showing any synchronization with hippocampal theta. *B* shows one example of the subgroup of non-HCN neurons ($n = 4$) characterized by irregular spiking during baseline periods and switched to theta bursting in response to tail pinch (similar to the tail pinch responsive subgroup of HCN-IR cells of which one example is shown on Fig. 4*B*). The neuron presented in *C* (the only one of this type) exhibited very low baseline activity and was activated by tail pinch. It fired spike clusters phase locked to every second theta wave. As a result, the dominant frequency component in its firing activity had half the frequency of ongoing hippocampal theta (compare the corresponding EEG and unit wavelets in the left column of part *C*). *D*, during ripples, the group of non-HCN neurons, similar to HCN-IR cells, did not show a characteristic direction of alteration in activity as can be seen on the left peri-event time histogram representing the firing activity of all non-HCN neurons ($n = 12$). However, on the level of individual cells both activation – middle histogram – and inhibition – right histogram – were observed. Bin size of peri-event time histograms: 10 ms.

exhibited theta bursting activity alike, the majority fired in an irregular, non-theta pattern.

HCN-IR neurons show a tendency to discharge at higher rate than HCN-immunonegative cells

Changes in the activity level of MS neurons during hippocampal state transitions are well documented (Ford *et al.* 1989). Therefore, the discharge rate of the recorded cells was determined across the distinguished hippocampal EEG states. In general, a tendency for higher activity of HCN-IR neurons (both PV and non-PV) compared to non-HCN cells was observed during each analysed hippocampal EEG pattern (non-theta, theta and ripple, see Table 1), but a significant 'anatomical group'–'hippocampal state' interaction could not be detected (repeated measures ANOVA and pairwise comparison of groups, $P > 0.05$, $n = 37$). By examining firing rate differences among hippocampal states in each anatomical group, a significantly higher level of activity was observed in the case of HCN/PV neurons during theta compared to non-theta periods (19.82 ± 6.15 Hz *versus* 12.02 ± 8.55 Hz; $P < 0.01$, $n = 14$).

Changes of the firing rate of cells during the formation of sharp wave ripples, known to affect the MS network (Dragoi *et al.* 1999), were also determined. The number of ripples varied considerably across experiments (median $\pm$ interquartile range: 20 ± 16; min–max: 5–52, $n = 37$ experiments) possibly due to the variable level of anaesthesia. All types of ripple-associated firing rate changes (activation, inhibition or no change) were observed independent of anatomical group. Ripples were accompanied by elevated firing activity in the case of eight HCN-IR (7 PV, 1 non-PV) and three non-HCN neurons (2 non-PV, 1 not tested). Nine neurons decreased their firing rate (5 HCN: 2 PV, 2 non-PV, 1 not tested; 4 non-HCN: 1 PV, 3 non-PV). Peri-event time histograms showing discharge activity of HCN-IR and non-HCN neurons during sharp wave ripples are presented on Figs 4*D* and 5*D*, respectively.

Taken together, the direction of firing rate change during state transitions was not a distinguishing characteristic of HCN-IR neurons, but a higher level of activity characterized these cells compared to non-HCN neurons across all hippocampal EEG states.

Phase relationship of the identified neurons to the hippocampal theta rhythm

Phase preference of the theta burst firing neurons to the ongoing hippocampal theta oscillation in the CA1 pyramidal layer was determined by calculating the cross-wavelet-based instantaneous phase-difference in the theta band between the EEG and the unit signal (Fig. 6 and Table 2 contain data for all neurons). All theta bursting neurons irrespective of anatomical identity showed a strong, unimodal phase preference evidenced by both high mean vector length (MVL: proportional to coupling strength) and Rao's spacing test (see the MVL in Table 2 and the concentration of dots representing neurons in a narrow band close to the periphery of the polar plot in Fig. 6*C*). Thus, statistically significant difference concerning coupling strength could not be detected either between theta bursting HCN-IR and non-HCN neurons (MVL: 0.95 ± 0.06 *versus* 0.94 ± 0.08; $P > 0.9$; $n = 24$ *versus* 4) or between the HCN-IR subgroups (PV-IR and non-PV: 0.95 ± 0.08 *versus* 0.94 ± 0.07; $P > 0.9$; $n = 14$ *versus* 7). Surprisingly, the population-level phase preference of the HCN-IR subgroups was proved to be significantly different (two sample Watson test, $n = 14$ *versus* 7, $P < 0.01$): the phase histogram of the PV-IR HCN subgroup was bimodal in contrast to the multimodal distribution of phase angles characterizing the non-PV HCN subgroup. Thus, overlapping with a previous study (Borhegyi *et al.* 2004), the population phase distribution of HCN/PV neurons could be fitted by the mixture of two von Mises probability density functions (mixing ratio: 0.54; error of estimate: 3.25×10^{-5}). The resulting mean angles representing the phase preference of the HCN/PV-neuron subgroups were 168.84 deg and 268.63 deg (Fig. 6*A* and *B*). The two subgroups could also be clearly distinguished on the polar plot, which shows the phase preference of all individual theta bursting cells. Tighter grouping of neurons around the trough (180 deg) indicated by a large concentration parameter (5.44) *versus* a more scattered distribution and low concentration parameter (3.70) of ascending phase-associated cells can also be observed on the phase histogram and polar plot of Fig. 6*B* and *C*, respectively). On the contrary, PV-negative HCN-IR neurons did not show group level phase preference despite having robust unimodal phase distribution individually (Fig. 6*B* and *C*). On the polar plot, these neurons distributed almost evenly around the unit circle. The robust difference in the group-level phase distribution of PV-IR and non-PV neurons was also indicated by the much higher population-level phase coupling of the former compared to the latter HCN-IR subgroup (HCN/PV population MVLs: 0.9 and 0.85 *versus* HCN/non-PV population MVL: 0.02, $n = 14$ *versus* 7, respectively). The small number of theta bursting HCN-immunonegative neurons ($n = 1$ PV-IR and 3 non-PV) did not allow the statistical comparison of mean angles with the HCN-IR groups. However, it is clearly visible on the polar plot representation that all but the single PV-IR neuron prefer to fire during phases that are non-overlapping with either group of HCN-IR cells. The HCN-immunonegative PV-IR neuron fired on the ascending phase, close to the peak of the theta cycle falling into one of the HCN/PV neuron groups.

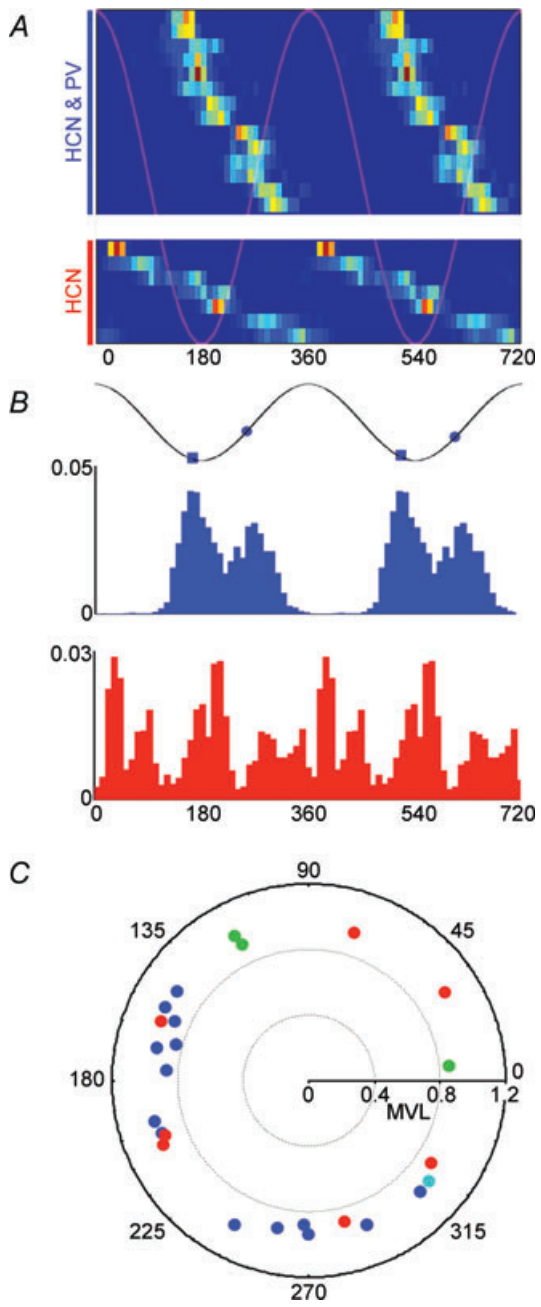

Figure 6. Phase relation of theta bursting neurons of the analysed anatomical groups to hippocampal theta activity
A, the phase histograms of neurons arranged in an ascending order of mean angles and merged into a matrix. Each row corresponds to an individual phase histogram. Two idealized theta cycles (in light purple) were overlaid for reference. Note that PV-containing HCN-IR neurons fire only on the ascending phase of the theta cycle and tend to form groups around the trough and before the peak of the cycle while the HCN-IR/non-PV group covers the entire cycle. *B*, the cumulative phase histograms of the two major anatomical groups. As demonstrated in *A* the bimodal distribution of PV/HCN-IR neurons as opposed to the multimodal distribution of HCN/non-PV phase angles is clearly visible. The Y-axis corresponds to firing probability. *C*, polar plot in which the individual phase preferences and mean vector length (MVL) are plotted for all theta bursting neurons. Larger distance from the centre of the circle means higher mean vector length value corresponding to stronger phase coupling. Note the grouping of PV-IR neurons (both HCN-IR = blue dots and non-HCN = cyan dot) around the trough (180 deg) and before the peak (360 deg) of the theta cycle. In contrast, non-PV/HCN neurons (red dots) are dispersed around the circle not showing a group-level phase preference. The three non-HCN/non-PV neurons (green dots) preferred to fire in regions avoided by the other anatomical groups. Bin size for phase histograms = 10 deg.

Effect of the local block of HCN channels on the firing activity of HCN-expressing neurons

In an attempt to uncover how HCN channels contribute to the regulation of firing activity of individual HCN-IR neurons, juxtacellular recording and labelling was combined with the local iontophoresis of h-current blockers to the vicinity of the recorded units, and the resulting changes in firing activity were analysed. The organic h-current blocker ZD7288 was iontophoretically applied in two different doses (0.5 and 5 mM, $n = 4$ and $n = 7$, respectively; see Methods and Supplemental material for details about the iontophoresis experiments). The effect of drug application on firing rate, theta modulation, theta burst activity and phase relation of medial septal unit activity to hippocampal theta was analysed. In order to examine the state dependence of the effect of ZD7288 on neuronal activity, non-theta periods and tail-pinch-induced theta segments were analysed separately. For the summary of effects of ZD7288 on tail pinch-induced theta-related firing activity see Supplementary Fig. 4.

First, it was tested whether the iontophoresis of ZD influences the frequency or power of hippocampal theta. Neither of these parameters was affected by local ZD application into the vicinity of the recorded MS neurons indicating the any effect of ZD iontophoresis on neuronal activity would arise from the local blockade of HCN channels (power – low/high dose: $P = 0.80/0.97$; frequency – low/high dose: $P = 0.30/0.11$, $n = 4$ and 7, Friedman's ANOVA).

From the 25 HCN-IR neurons included in this study, 11 neurons were subjected to ZD7288 iontophoresis. Ten out of these 11 neurons exhibited a theta bursting pattern during hippocampal theta periods, five even during non-theta segments. Large variability of firing activity was observed during both the control and drug application periods especially in the case of the recordings with the low ZD dose. The most affected characteristic of unit activity by ZD application was proved to be firing rate.

Firing rate – non-theta. Drug iontophoresis resulted in a gradual but not strictly monotonic decrease of firing rate interrupted by elevations around hippocampal state transitions (non-theta to theta and vice versa) in case

Table 2. Phase preference of theta bursting neurons

Cell code	Phase (deg)	Mean vector length
HCN/PV		
378n1/T	156	0.89
393n1/T	195	0.97
506n1/T	153	0.98
528n2/T	200	0.95
691n4/T	168	0.95
698n1/T	165	0.84
706n1/T	176	0.87
730n2/T	146	0.97
583n3/AP	258	0.92
631n3/AP	270	0.94
632n1/AP	315	0.96
701n1/AP	292	0.95
708n2/AP	243	0.99
729n2/AP	268	0.88
HCN/NT		
327n2	357	0.96
431n1	251	0.97
451n3	131	0.92
HCN/non-PV		
390n4	73	0.94
449n1	158	0.97
604n2	33	0.99
624n1	201	0.94
626n1	284	0.89
645n1	204	0.97
704n1	326	0.9
PV/non-HCN		
728n2/T	320	0.96
non-HCN/non-PV		
331n4	116	0.92
361n2	117	0.99
391n1	6	0.86

Phase = circular mean; T: trough-preferring group (mean: 168.84 deg), AP: ascending phase, peak-preferring group (mean: 268.63 deg). NT: not tested for PV.

of three cells from the low ($n = 4$) and four cells from the high dose group ($n = 7$). The suppressing effect on neuronal activity was proved to be significant in two low dose and three high dose cases by Friedman's ANOVA (time as the dependent variable; $P < 0.05$). However, significant dose–time interaction was not observed (by repeated measures ANOVA at $P = 0.05$). Concerning the time course of the ZD effect, significant suppression was detected starting at 642 and 254 s after the onset of drug administration with the low and from 148, 261 and 535 s with the high ZD dose while the maximal magnitude of firing rate decrease reached 71.4% and 88.4% (low dose) and 69.8%, 95.7% and 96.2% (high dose, see the neuron in Fig. 7). In one neuron, a gradual and significant increase was found during the application of the low ZD dose. A similar effect (elevation of activity) characterized two high dose neurons as well. Rise in discharge level started at 431 s (low), but at 254 and 392 s (high) during drug injection and reached 116.7% (low) and 236.4–247.2% of control (high), respectively.

Firing rate – theta. The direction of drug effect (suppression, elevation or no change of discharge frequency) on theta-associated firing activity was similar to that registered during non-theta periods but the magnitude was smaller. Accordingly, reduction was observed in the case of three low and three high dose neurons but reached significance only in one high dose cell (13.88% decrease in firing rate compared to control during the theta period lasting from 305 to 332 s after ZD injection onset, see Fig. 7).

Firing pattern – theta-content of unit activity. Surprisingly, the theta-rhythmic activity of HCN neurons was not affected significantly by h-current blockade. Thus, consistent changes of the theta content of unit activity were not observed in response to ZD7288 iontophoresis except in case of one neuron which belonged to the subgroup of constitutive bursting cells (shown in Fig. 7). Both the baseline and hippocampal theta-associated rhythmic activity of this neuron were suppressed but not attenuated during drug application. It should be noted that the firing rate suppressing effect of ZD application was the strongest in the case of this neuron.

Firing pattern – characteristics of theta bursts. Although none of the burst parameters (frequency of theta burst generation, number of spikes in bursts, burst length, intraburst frequency) were affected significantly by ZD administration, a tendency of concurrent intraburst spike number and burst length reduction during the application of the high ZD dose should be noted (intraburst spike number from 4.76 ± 3.78 to 3.13 ± 0.72; burst length: from 80.25 ± 36.7 ms to 48.4 ± 13.1 ms, comparison of pre-drug and 15 min post-drug periods: $P = 0.6$ and 0.1, $n = 7$ *versus* 3 in both cases).

Phase preference. The phase relationship to hippocampal theta remained stable during drug iontophoresis except in two neurons (1 low and 1 high dose neuron, the latter shown on Fig. 7). In these cases major shifts from control phase preference (low neuron – 2 control *versus* 2 drug theta periods: 307 deg and 328 deg, ZD: 41.2 deg and 36.7 deg; high neuron: 292 deg and 301 deg *versus* 99.1 deg and 346 deg) were detected without change or only a slight decrease in coupling strength (mean vector length: low: 0.99 *versus* 0.97; high: 0.92 *versus* 0.83, see Fig. 7*G*). The firing rate of both of

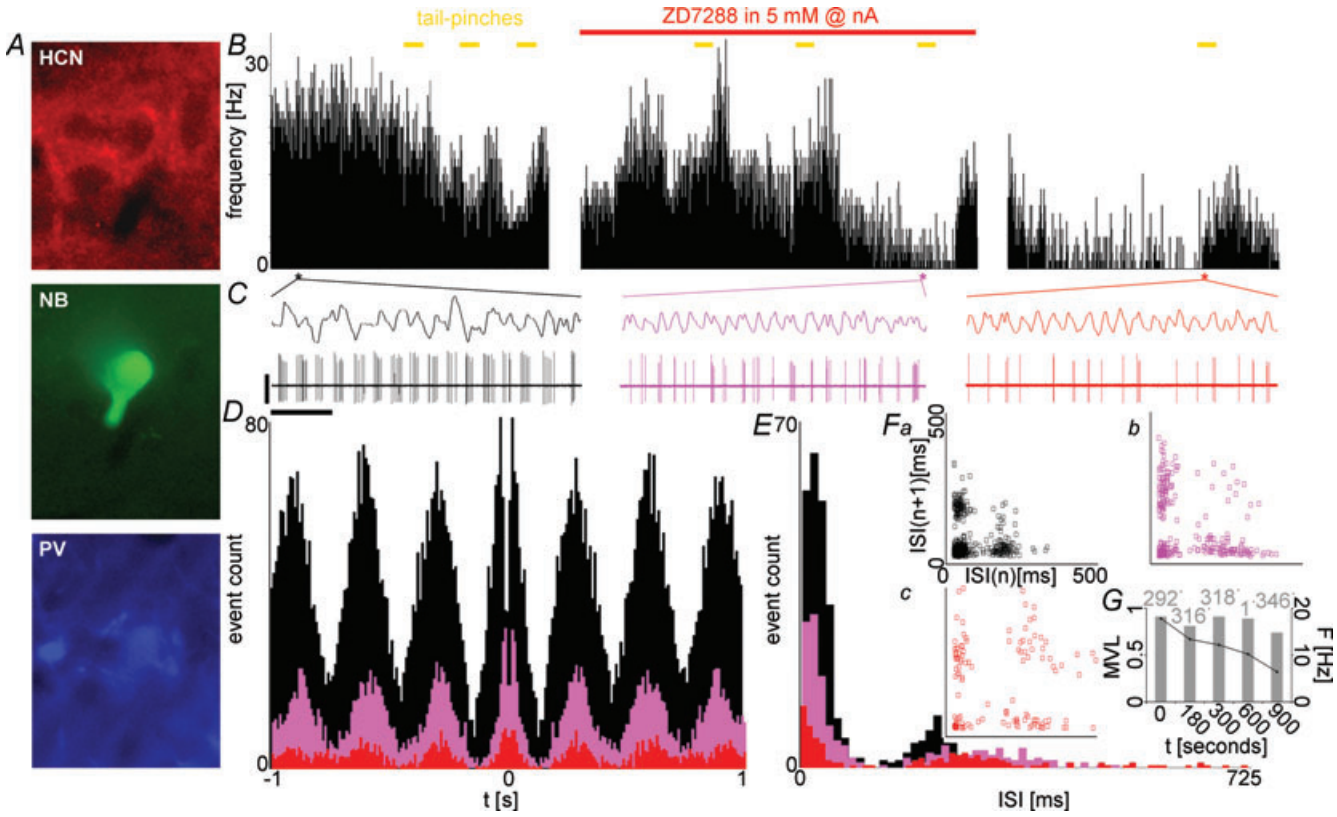

Figure 7. The local blockade of HCN channels in the vicinity of an HCN-IR neuron causes robust reduction of firing activity without disrupting theta-modulated discharge

A, fluorescence photomicrographs in which the immunocytochemical identification is demonstrated. As shown, this neuron was proved to express both HCN and PV. *B*, plot of the firing rate of the neuron during the control and drug injection periods counted in 1 s windows. Note the reduction of firing around the half of the control recording period coincident with the cessation of spontaneous theta in the hippocampus (not shown). The intermittent elevations following tail pinches (yellow bars = 30 s) can also be observed. The application of the HCN blocker ZD7288 (red line) at 5 mM at 40 nA had resulted in a gradual reduction of firing activity falling well below control level which continued after the cessation of ZD ejection. The latter phenomenon could be explained by the well-documented irreversible nature of HCN blockade by ZD (see Results for reference). *C*, three 5 s long segments are shown separately cut from spontaneous weak (left trace) or tail-pinch-elicited strong theta episodes (middle trace and right trace). The location of the selected segments are marked by * (it should be noted that the width of the asterisks corresponds to ~5 s). It is clearly visible that the length of theta bursts is decreased due to the reduction in the number of spikes per bursts. Coincidentally, the number of omitted theta cycles was increased resulting in the lengthening of interburst intervals. Note that before the onset of drug ejection the neuron fired in theta burst mode even when theta was weak in the hippocampus (this cell belonged to the constitutively bursting HCN-IR neuron group: see the mixed slow oscillatory/theta-like pattern of the EEG and the highly regular theta bursting of the MS unit on the left trace). It is also clearly visible that hippocampal theta was not affected by ZD microiontophoresis (compare the EEG on the middle and right trace). The robust drop in firing rate with concurrent stability of the bursting pattern is also evident on the autocorrelograms of panel *D* calculated from the theta episodes sampled for panel *C*. The lowering of intraburst spike number is proven by the drop in the height of the first peak of the interspike interval histogram of panel *E* corresponding to intraburst intervals. Panel *Fa–c* shows the recurrence plots of interspike intervals on which the intra- (next to the origo) and interburst intervals (further along the two axes) are clearly separated. The fourth cluster of intervals represents single spikes occurring outside theta bursts. Note that the proportion of the latter relative to intraburst intervals increased during drug ejection indicating that theta bursts were replaced partly by single spikes. *G*, the phase relationship of firing to the ongoing theta was shifted (mean angles above columns), but the strength of phase preference did not change consistently (MVL: mean vector length on left axis, and grey columns) despite the significant drop of firing activity (*F*: firing rate on right axis and black line plot). Horizontal bar below raw traces = 1 s, vertical bar = 2 mV for unit and 0.7 mV for EEG. Bin size for autocorrelogram = 10 ms; for ISIH plots = 1 ms.

these neurons was significantly affected by ZD injection and one of them (the high) belonged to the constitutively bursting HCN-IR subgroup. The theta modulation of the latter neuron was also significantly reduced (see the section about ZD effect on theta content).

Discussion

Main findings

We have demonstrated that (i) HCN channels are highly abundant in the medial septum and are localized in the soma-dendritic membrane of GABAergic neurons; (ii) a subpopulation of HCN-IR neurons projects to the hippocampus and contains parvalbumin; (iii) HCN expression robustly correlated with theta rhythmic firing, e.g. a significant theta frequency component was present in the firing pattern of all HCN-IR neurons, whereas only the minority of non-HCN neurons exhibited theta-related firing pattern; (iv) all theta bursting neurons were tightly phase coupled to hippocampal theta but only PV-containing HCN neurons showed group-level phase preference. In contrast, the PV-negative HCN-IR subgroup covered the entire theta cycle despite strong individual phase coupling; and (v) the main effect of blocking h-current locally reduced the firing rate of HCN-IR neurons without disrupting theta-modulated firing.

Technical considerations

The number of theta rhythmic neurons in this study is larger than theta-unrelated cells. The biological reason may be the tight association of the MS network with theta genesis indicating that a large part of this brain region exhibits theta-modulated firing activity. This claim is supported by several single unit recording studies of the medial septum in which the majority of recorded neurons showed theta-modulated discharge activity (Alonso *et al.* 1987; Ford *et al.* 1989). However, the effect of anaesthesia on neuronal activity (Sweeney *et al.* 1992) and difference in the sensitivity of neurons to the juxtacellular labelling method can also lead to biased sampling (the ability of neurons to survive after the labelling procedure can vary; Pinault, 1996). Thus, the postlabelling survival time was reduced to increase the probability of successful recovery of labelled cells (both theta bursting and non-bursting).

Neurochemical identity of HCN-IR neurons

All of the HCN-expressing cells including septo-hippocampal projection neurons were found to be GABAergic, with a subset also containing parvalbumin. This finding is in line with mounting evidence indicating that the GABAergic network is the main source of theta rhythmic drive in the medial septum. It was shown that fast spiking neurons capable of theta burst generation express the GABA synthesizing enzyme GAD67, and respond to hyperpolarizing current injection with a profound depolarizing sag indicative of h-current (Sotty *et al.* 2003). Moreover, theta bursting neurons recorded both in the anaesthetized and in the drug-free rats were shown to be GABAergic (Simon *et al.* 2006). Thus, the presence of HCN channels would distinguish the theta-rhythmic subpopulation of GABAergic neurons in the MS. On the other hand, theta burst pattern was exhibited by some HCN-negative neurons as well. One non-HCN cell even produced low frequency bursting coupled to hippocampal theta. In these neurons rhythmic activity could be entrained by another HCN-subunit (HCN4), not studied here, by other pacemaker channels, or by rhythmic network inputs indicating that multiple rhythm-generating mechanisms may function in parallel in the MS as shown for other pattern generator circuitries (Thoby-Brisson & Ramirez, 2001). Of course, false-negative staining for HCN1 or HCN2 of the juxtacellularly labelled neurons cannot be excluded either.

Difference between PV-IR and PV-negative HCN-subgroups in phase relationship to hippocampal theta rhythm

Neurons in an oscillating network fire at a characteristic phase of the background oscillation. The phase preferred by a given neuron group provides important clues about their role in generating the given oscillatory activity pattern (Ujfalussy & Kiss, 2006). Thus, the phase relationship of theta bursting neurons in this study to hippocampal theta was calculated. All theta bursting neurons exhibited robust unimodal phase preference, but a very significant difference was found between the PV-IR and non-PV HCN subgroups: the former was characterized by a bimodal phase distribution whereas the latter did not concentrate at any unique phase of the theta cycle. Hence, in agreement with our previous study, the phase distribution of PV-containing HCN-IR neurons had peaks around the trough and on the ascending phase, before the peak of CA1 pyramidal layer theta (Borhegyi *et al.* 2004). It should also be noted that, based on phase preference, the only PV-IR non-HCN neuron fell into one of the HCN/PV-IR groups, which strengthens the observation that PV immunoreactivity correlates with characteristic phase preference. However, the ascending phase group of PV-IR neurons was found to be less stable, indicated by the lower and broader peak in the phase histogram.

Our data raise two possibilities: (i) the output of the MS GABAergic neuron network is composed of multiple

phases covering the entire theta cycle; (ii) different neurochemical classes of this network have characteristic phase relationships to hippocampal theta. It is known that the MS projects to virtually all limbic areas (of which the most prominent connection is established with the hippocampus) where rhythmic neurons in phase relation with hippocampal theta were found (Dickson *et al.* 1995; Kocsis & Vertes, 1997). Therefore, the medial septal phase diversity is paralleled by that observed in the targets of the GABAergic MS pathway including the hippocampal interneuron network (Somogyi & Klausberger, 2005).

The firing behaviour of HCN-IR neurons

The firing pattern of all HCN-IR neurons contained a significant theta frequency component, whereas the same could be found only in the third of non-HCN cells. It should be emphasized that HCN channels were localized in the soma-dendritic membranes of medial septal neurons, whereas HCN-bearing axon terminals were rare. Thus, h-current may be critical in determining the membrane potential of the soma-dendritic region (Sekirnjak & du Lac, 2002; Nolan *et al.* 2004; Nolan *et al.* 2007; Tan *et al.* 2007), and consequently the firing pattern of HCN-IR MS neurons. The HCN channel has been known for decades as the prototypical pacemaker channel (Robinson & Siegelbaum, 2003). Its role in the generation of spontaneous membrane potential oscillations and rhythmic action potential genesis was conclusively demonstrated (Bennett *et al.* 2000; Dickson *et al.* 2000; Wilson, 2005). Furthermore, the ability of various neurons to be selectively entrained by theta frequency input was also connected to the presence of h-current in them (Hu *et al.* 2002). The indispensability of HCN channels for theta rhythm genesis was also demonstrated beyond the single cell level in the hippocampal slice preparation (Cobb *et al.* 2003). It was also shown that HCN expression can be a distinguishing characteristic of certain neuron types connected to rhythm genesis (Cooper & Stanford, 2000; Neuhoff *et al.* 2002). Remarkably, in a subpopulation of HCN-IR neurons in this study, hippocampal theta-independent theta bursting was observed. It may indicate the presence of spontaneous, theta frequency oscillation in these cells as previously described (Ford *et al.* 1989; Barrenechea *et al.* 1995). Based on the ability to produce theta rhythmic activity in the lack of hippocampal theta, these neurons were thought to be the pacemakers of MS theta-genesis (Petsche *et al.* 1962; Wang, 2002). Thus, the presence of HCN channels may distinguish the putative pacemaker population of the MS network.

The analysis of both the power and duration of theta rhythmic activity of HCN-IR neurons revealed substantial heterogeneity in the extent of theta-dominance in their firing pattern, which is paralleled by the variability in the intensity of immunoreaction on both the fluorescence and electron-microscopic levels. Direct correlation between the number of HCN channels and firing pattern could not be investigated since the juxtacellular labelling can cause long-lasting depolarization along with changes of the intracellular ion milieu leading to modification of HCN function (Fan *et al.* 2005). Hence, HCN immunocytochemistry in the physiological experiments was used solely for deciding whether the recorded neuron was HCN positive or negative. Nevertheless, the observed heterogeneity of both theta rhythmicity and HCN immunoreactivity could be explained by the complex regulation of HCN channel function involving second messenger modulation that can alter the amplitude and frequency of subthreshold oscillations (Luthi & McCormick, 1998*b*; Wang *et al.* 2002; Zolles *et al.* 2006). In turn, it can result in changes in theta induction threshold, and variability of theta dominance of firing pattern. Additionally, variability in HCN expression may lead to diverse staining intensity patterns as was conclusively shown by immunoelectron microscopy.

The observed higher firing frequency of HCN-IR neurons compared to non-HCN cells could be caused by the depolarizing effect of h-current. A significant proportion of HCN channels can be in the active state around the resting membrane potential depending upon the intracellular second messenger concentration. A possible source of the critical second messengers keeping a significant depolarizing ion flow through HCN channels may be the massive neuromodulatory inputs of the MS (Segal, 1976). Moreover, besides neuromodulatory influences, the robust GABAergic tone originating partly from the MS GABAergic network can also contribute to the activation of h-current by lowering the membrane potential into the activation range of HCN channels (Henderson *et al.* 2004).

Effect of HCN-blockade on firing activity

The main findings of iontophoresis experiments were the reduction of firing activity without the cessation of theta rhythmicity in response to h-current blockade by ZD7288 application. In these recordings the large variability and resulting low level of significance may have both technical and physiological reasons. A large fluctuation of the response to ZD7288 iontophoresis was also observed in the *in vitro* pilot recordings under more tightly controlled conditions compared to those achievable in experiments *in vivo* (details of the *in vitro* experiments are provided in the Supplemental material). The electrode design-related variability, which is discussed in the Supplemental material, combined with the uncontrollability of the tissue surroundings of the tip of the iontophoresis pipette during drug injection, could also increase the range of possible outcomes of drug

application. The observed diversity of responses could have at least two biological sources. The already mentioned complexity of HCN channel regulation would produce a heterogeneous set of HCN channels with various activity states. Hence, the drug effect on HCN-mediated processes could vary considerably. Additionally, the state of the network impinging upon the neuron can considerably fluctuate under urethane anaesthesia (Dickson *et al.* 2007). Despite these difficulties a clear-cut effect of HCN-blockade was detected in the form of a suppression of firing activity possibly due to the attenuation of the depolarizing influence of HCN channels. The latter claim is supported by previous data showing hyperpolarization and a modest decrease of firing rate of globus pallidus GABAergic neurons recorded *in vitro* in response to ZD7288 (Chan *et al.* 2004). Moreover, the rebound spiking of MS neurons evoked by the rhythmic stimulation of hippocampo-septal fibres was blocked by ZD7288 application in slice preparation (Manseau *et al.* 2008). Remarkably, the block of HCN channels slightly altered but did not eliminate theta rhythmicity in our recordings. These results are in agreement with a previous study demonstrating a decrease in the frequency without the cessation of hippocampal theta in response to HCN-blockade in the MS (Kocsis & Li, 2004). The preservation of theta rhythmic firing of HCN neurons might be traced to two possible causes. First, MS GABAergic neurons are heavily interconnected and may mutually drive each other's rhythmicity (Henderson *et al.* 2004). Second, cell-autonomous oscillation can be determined by other channels besides HCN (for a review see Ramirez *et al.* 2004). Hence, the pharmacologically eliminated pacemaker HCN channels could be replaced by theta rhythmic inputs and unaffected ionic mechanisms. It should also be noted that in the case of some neurons (i.e. that shown in Fig. 7) the change in firing activity continued after switching off ZD iontophoresis. This observation can be explained by the well-known irreversibility of HCN blockade by ZD (Gasparini & Difrancesco, 1997). In summary, iontophoresis experiments imply that HCN channels may contribute to the theta rhythmic firing of MS GABAergic neurons by shifting the membrane potential to more depolarized values.

Possible role of HCN-IR neurons in MS theta genesis

Since HCN channels are targeted by various signal transduction cascades via the direct action of second messenger molecules (Luthi & McCormick, 1998*b*; Wang *et al.* 2002; Zolles *et al.* 2006), theta genesis in the MS can be finely regulated by inputs converging on the HCN-IR GABAergic neurons. This claim is supported by the following discoveries: MS GABAergic neurons of which the theta bursting subgroup may express HCN are decorated by a unique set of metabotropic transmitter receptors (Alreja, 1996; Alreja *et al.* 2000*a*,*b*; Wu *et al.* 2002, 2003; Luttgen *et al.* 2004; Xu *et al.* 2004; Bassant *et al.* 2005; Luttgen *et al.* 2005), all of which can modulate HCN function. Elevation of cAMP in MS neurons has the opposite effect to HCN blockade, i.e. increase of hippocampal theta frequency (Kocsis & Li, 2004) or induction of theta burst firing (Fitch *et al.* 2006). On the contrary, decrease of cAMP level by the G_i-coupled somatostatin-2A receptor resulted in the reduction of firing activity and theta bursting (Bassant *et al.* 2005), which resembled that observed in our study in response to HCN blockade.

In summary, HCN neurons may be critical components of the theta-generating network in the MS converting a multicomponent neurochemical signal converging on HCN channels into a theta patterned output which then synchronizes the septo-hippocampal circuitry.

References

Alonso A, Gaztelu JM, Buno W Jr & Garcia-Austt E (1987). Cross-correlation analysis of septohippocampal neurons during theta rhythm. *Brain Res* **413**, 135–146.

Alreja M (1996). Excitatory actions of serotonin on GABAergic neurons of the medial septum and diagonal band of Broca. *Synapse* **22**, 15–27.

Alreja M, Shanabrough M, Liu W & Leranth C (2000*a*). Opioids suppress IPSCs in neurons of the rat medial septum/diagonal band of Broca: involvement of μ-opioid receptors and septohippocampal GABAergic neurons. *J Neurosci* **20**, 1179–1189.

Alreja M, Wu M, Liu W, Atkins JB, Leranth C & Shanabrough M (2000*b*). Muscarinic tone sustains impulse flow in the septohippocampal GABA but not cholinergic pathway: implications for learning and memory. *J Neurosci* **20**, 8103–8110.

Barrenechea C, Pedemonte M, Nunez A & Garcia-Austt E (1995). In vivo intracellular recordings of medial septal and diagonal band of Broca neurons: relationships with theta rhythm. *Exp Brain Res* **103**, 31–40.

Bassant MH, Simon A, Poindessous-Jazat F, Csaba Z, Epelbaum J & Dournaud P (2005). Medial septal GABAergic neurons express the somatostatin sst2A receptor: functional consequences on unit firing and hippocampal theta. *J Neurosci* **25**, 2032–2041.

Bennett BD, Callaway JC & Wilson CJ (2000). Intrinsic membrane properties underlying spontaneous tonic firing in neostriatal cholinergic interneurons. *J Neurosci* **20**, 8493–8503.

Borhegyi Z, Varga V, Szilagyi N, Fabo D & Freund TF (2004). Phase segregation of medial septal GABAergic neurons during hippocampal theta activity. *J Neurosci* **24**, 8470–8479.

Buzsaki G (2002). Theta oscillations in the hippocampus. *Neuron* **33**, 325–340.

Chan CS, Shigemoto R, Mercer JN & Surmeier DJ (2004). HCN2 and HCN1 channels govern the regularity of autonomous pacemaking and synaptic resetting in globus pallidus neurons. *J Neurosci* **24**, 9921–9932.

Cobb SR, Larkman PM, Bulters DO, Oliver L, Gill CH & Davies CH (2003). Activation of I_h is necessary for patterning of mGluR and mAChR induced network activity in the hippocampal CA3 region. *Neuropharmacology* **44**, 293–303.

Cooper AJ & Stanford IM (2000). Electrophysiological and morphological characteristics of three subtypes of rat globus pallidus neurone *in vitro*. *J Physiol* **527**, 291–304.

Dickson CT, Kirk IJ, Oddie SD & Bland BH (1995). Classification of theta-related cells in the entorhinal cortex: cell discharges are controlled by the ascending synchronizing pathway in parallel with hippocampal theta-related cells. *Hippocampus* **5**, 306–319.

Dickson CT, Lo AS, Clement EA, Mah ET & Richard A (2007). Cyclical and sleep-like alternations of brain state are specific to urethane anaesthesia. *2007 Abstract Viewer/Itinerary Planner*, Program No. 791.3. Society for Neuroscience, Washington, DC.

Dickson CT, Magistretti J, Shalinsky MH, Fransen E, Hasselmo ME & Alonso A (2000). Properties and role of I_h in the pacing of subthreshold oscillations in entorhinal cortex layer II neurons. *J Neurophysiol* **83**, 2562–2579.

Dragoi G, Carpi D, Recce M, Csicsvari J & Buzsáki G (1999). Interactions between hippocampus and medial septum during sharp waves and theta oscillation in the behaving rat. *J Neurosci* **19**, 6191–6199.

Dwyer TA, Servatius RJ & Pang KC (2007). Noncholinergic lesions of the medial septum impair sequential learning of different spatial locations. *J Neurosci* **27**, 299–303.

Fan Y, Fricker D, Brager DH, Chen X, Lu HC, Chitwood RA & Johnston D (2005). Activity-dependent decrease of excitability in rat hippocampal neurons through increases in I_h. *Nat Neurosci* **8**, 1542–1551.

Fisher NI (1993). *Statistical Analysis of Circular Data*. Cambridge University Press, Cambridge, UK.

Fitch TE, Sahr RN, Eastwood BJ, Zhou FC & Yang CR (2006). Dopamine D1/5 receptor modulation of firing rate and bidirectional theta burst firing in medial septal/vertical limb of diagonal band neurons in vivo. *J Neurophysiol* **95**, 2808–2820.

Ford RD, Colom LV & Bland BH (1989). The classification of medial septum-diagonal band cells as theta-on or theta-off in relation to hippocampal EEG states. *Brain Res* **493**, 269–282.

Freund TF & Antal M (1988). GABA-containing neurons in the septum control inhibitory interneurons in the hippocampus. *Nature* **336**, 170–173.

Gasparini S & Difrancesco D (1997). Action of the hyperpolarization-activated current (I_h) blocker ZD7288 in hippocampal CA1 neurons. *Pflugers Arch* **435**, 99–106.

Gerashchenko D, Salin-Pascual R & Shiromani PJ (2001). Effects of hypocretin-saporin injections into the medial septum on sleep and hippocampal theta. *Brain Res* **913**, 106–115.

Henderson Z, Fiddler G, Saha S, Boros A & Halasy K (2004). A parvalbumin-containing, axosomatic network in the rat medial septum: relevance to rhythmogenesis. *Eur J Neurosci* **19**, 2753–2768.

Hu H, Vervaeke K & Storm JF (2002). Two forms of electrical resonance at theta frequencies, generated by M-current, h-current and persistent Na^+ current in rat hippocampal pyramidal cells. *J Physiol* **545**, 783–805.

Kiss J, Patel AJ, Baimbridge KG & Freund TF (1990). Topographical localization of neurons containing parvalbumin and choline acetyltransferase in the medial septum-diagonal band region of the rat. *Neuroscience* **36**, 61–72.

Klausberger T, Magill PJ, Márton LF, Roberts JD, Cobden PM, Buzsáki G & Somogyi P (2003). Brain-state- and cell-type-specific firing of hippocampal interneurons in vivo. *Nature* **421**, 844–848.

Kocsis B & Li S (2004). In vivo contribution of h-channels in the septal pacemaker to theta rhythm generation. *Eur J Neurosci* **20**, 2149–2158.

Kocsis B & Vertes RP (1997). Phase relationship of rhythmic neuronal firing in the supramammillary nucleus and mammillary body to the hippocampal theta activity in the urethane anesthetized rats. *Hippocampus* **7**, 204–214.

Kosaka T, Kosaka K, Tateishi K, Hamaoka Y, Yanaihara N, Wu JY & Hama K (1985). Gabaergic neurons containing the CCK-8-like and/or VIP-like immunoreactivities in the rat hippocampus and dentate gyrus. *J Comp Neurol* **239**, 420–430.

Li X, Yao X, Fox J & Jefferys JG (2007). Interaction dynamics of neuronal oscillations analyzed using wavelet transforms. *J Neurosci Methods* **160**, 178–185.

Luthi A & McCormick DA (1998*a*). H-current: properties of a neuronal and network pacemaker. *Neuron* **21**, 9–12.

Luthi A & McCormick DA (1998*b*). Periodicity of thalamic synchronized oscillations: the role of Ca^{2+}-mediated upregulation of Ih. *Neuron* **20**, 553–563.

Luttgen M, Ogren SO & Meister B (2005). 5-HT1A receptor mRNA and immunoreactivity in the rat medial septum/diagonal band of Broca-relationships to GABAergic and cholinergic neurons. *J Chem Neuroanat* **29**, 93–111.

Luttgen M, Ove Ogren S & Meister B (2004). Chemical identity of 5-HT2A receptor immunoreactive neurons of the rat septal complex and dorsal hippocampus. *Brain Res* **1010**, 156–165.

Manseau F, Goutagny R, Danik M & Williams S (2008). The hippocamposeptal pathway generates rhythmic firing of GABAergic neurons in the medial septum and diagonal bands: an investigation using a complete septohippocampal preparation *in vitro*. *J Neurosci* **28**, 4096–4107.

Morris NP, Fyffe RE & Robertson B (2004). Characterisation of hyperpolarization-activated currents (I_h) in the medial septum/diagonal band complex in the mouse. *Brain Res* **1006**, 74–86.

Neuhoff H, Neu A, Liss B & Roeper J (2002). I_h channels contribute to the different functional properties of identified dopaminergic subpopulations in the midbrain. *J Neurosci* **22**, 1290–1302.

Nolan MF, Dudman JT, Dodson PD & Santoro B (2007). HCN1 channels control resting and active integrative properties of stellate cells from layer II of the entorhinal cortex. *J Neurosci* **27**, 12440–12451.

Nolan MF, Malleret G, Dudman JT, Buhl DL, Santoro B, Gibbs E, Vronskaya S, Buzsaki G, Siegelbaum SA, Kandel ER & Morozov A (2004). A behavioral role for dendritic integration: HCN1 channels constrain spatial memory and plasticity at inputs to distal dendrites of CA1 pyramidal neurons. *Cell* **119**, 719–732.

Notomi T & Shigemoto R (2004). Immunohistochemical localization of I_h channel subunits, HCN1–4, in the rat brain. *J Comp Neurol* **471**, 241–276.

Paxinos G & Watson C (1998). *The Rat Brain in Stereotaxic Coordinates*, 4th edn. Academic Press, New York.

Petsche H, Stimpf C & Gogolak G (1962). The significance of the rabbit's septum as a relay between the midbrain and the hippocampus. I. The control of hippocampus arousal activity by the septum cells. *Electroencephalogr Clin Neurophysiol* **14**, 202–211.

Pinault D (1996). A novel single-cell staining procedure performed in vivo electrophysiological control: morpho-functional features of juxtacellularly labeled thalamic cells and other central neurons with biocytin or Neurobiotin. *J Neurosci Methods* **65**, 113–136.

Ramirez JM, Tryba AK & Pena F (2004). Pacemaker neurons and neuronal networks: an integrative view. *Curr Opin Neurobiol* **14**, 665–674.

Robinson RB & Siegelbaum SA (2003). Hyperpolarization-activated cation currents: from molecules to physiological function. *Annu Rev Physiol* **65**, 453–480.

Roux SG, Cenier T, Garcia S, Litaudon P & Buonviso N (2007). A wavelet-based method for local phase extraction from a multi-frequency oscillatory signal. *J Neurosci Methods* **160**, 135–143.

Rozen S & Skaletsky H (2000). Primer3 on the WWW for general users and for biologist programmers. *Methods Mol Biol* **132**, 365–386.

Segal M (1976). Brain stem afferents to the rat medial septum. *J Physiol* **261**, 617–631.

Sekirnjak C & du Lac S (2002). Intrinsic firing dynamics of vestibular nucleus neurons. *J Neurosci* **22**, 2083–2095.

Serafin M, Williams S, Khateb A, Fort P & Muhlethaler M (1996). Rhythmic firing of medial septum non-cholinergic neurons. *Neuroscience* **75**, 671–675.

Simon AP, Poindessous-Jazat F, Dutar P, Epelbaum J & Bassant MH (2006). Firing properties of anatomically identified neurons in the medial septum of anesthetized and unanesthetized restrained rats. *J Neurosci* **26**, 9038–9046.

Somogyi P & Klausberger T (2005). Defined types of cortical interneurone structure space and spike timing in the hippocampus. *J Physiol* **562**, 9–26.

Sotty F, Danik M, Manseau F, Laplante F, Quirion R & Williams S (2003). Distinct electrophysiological properties of glutamatergic, cholinergic and GABAergic rat septohippocampal neurons: novel implications for hippocampal rhythmicity. *J Physiol* **551**, 927–943.

Sweeney JE, Lamour Y & Bassant MH (1992). Arousal-dependent properties of medial septal neurons in the unanesthetized rat. *Neuroscience* **48**, 353–362.

Tan ML, Theeuwes HP, Feenstra L & Borst JG (2007). Membrane properties and firing patterns of inferior colliculus neurons: an in vivo patch-clamp study in rodents. *J Neurophysiol* **98**, 443–453.

Thoby-Brisson M & Ramirez JM (2001). Identification of two types of inspiratory pacemaker neurons in the isolated respiratory neural network of mice. *J Neurophysiol* **86**, 104–112.

Torrence C & Compo GP (1998). A practical guide to wavelet analysis. *Bull Am Meteor Soc* **79**, 61–78.

Toth K, Freund TF & Miles R (1997). Disinhibition of rat hippocampal pyramidal cells by GABAergic afferents from the septum. *J Physiol* **500**, 463–474.

Ujfalussy B & Kiss T (2006). How do glutamatergic and GABAergic cells contribute to synchronization in the medial septum? *J Comput Neurosci* **21**, 343–357.

Wang XJ (2002). Pacemaker neurons for the theta rhythm and their synchronization in the septohippocampal reciprocal loop. *J Neurophysiol* **87**, 889–900.

Wang J, Chen S, Nolan MF & Siegelbaum SA (2002). Activity-dependent regulation of HCN pacemaker channels by cyclic AMP: signaling through dynamic allosteric coupling. *Neuron* **36**, 451–461.

Wang M, Ramos BP, Paspalas CD, Shu Y, Simen A, Duque A, Vijayraghavan S, Brennan A, Dudley A, Nou E, Mazer JA, McCormick DA & Arnsten AF (2007). α2A-Adrenoceptors strengthen working memory networks by inhibiting cAMP-HCN channel signaling in prefrontal cortex. *Cell* **129**, 397–410.

Wilson CJ (2005). The mechanism of intrinsic amplification of hyperpolarizations and spontaneous bursting in striatal cholinergic interneurons. *Neuron* **45**, 575–585.

Wu M, Newton SS, Atkins JB, Xu C, Duman RS & Alreja M (2003). Acetylcholinesterase inhibitors activate septohippocampal GABAergic neurons via muscarinic but not nicotinic receptors. *J Pharmacol Exp Ther* **307**, 535–543.

Wu M, Zhang Z, Leranth C, Xu C, van den Pol AN & Alreja M (2002). Hypocretin increases impulse flow in the septohippocampal GABAergic pathway: implications for arousal via a mechanism of hippocampal disinhibition. *J Neurosci* **22**, 7754–7765.

Xu C, Michelsen KA, Wu M, Morozova E, Panula P & Alreja M (2004). Histamine innervation and activation of septohippocampal GABAergic neurones: involvement of local ACh release. *J Physiol* **561**, 657–670.

Yoder RM & Pang KC (2005). Involvement of GABAergic and cholinergic medial septal neurons in hippocampal theta rhythm. *Hippocampus* **15**, 381–392.

Zolles G, Klocker N, Wenzel D, Weisser-Thomas J, Fleischmann BK, Roeper J & Fakler B (2006). Pacemaking by HCN channels requires interaction with phosphoinositides. *Neuron* **52**, 1027–1036.

Acknowledgements

We would like to thank for excellent technical assistance Katalin Lengyel, Emõke Simon and Gyõzõ Goda. We are also grateful to Drs György Buzsáki and Bernát Kocsis for the critical reading of an earlier version of the manuscript, to Dr László Acsády for helping to complete the current version of the manuscript and to Rita Nyilas for her suggestions about the supplemental material. This work was supported by the grants OTKA K60927, the Howard Hughes Medical Institute (T.F.F.) and NIH MH54671 (T.F.F.); I.K. and V.V. were János Bolyai Research Fellows.

Supplemental material

Online supplemental material for this paper can be accessed at: http://jp.physoc.org/cgi/content/full/jphysiol.2008.155242/DC1